



Developments in proton MR spectroscopic imaging of prostate cancer

Angeliki Stamatelidou¹ · Tom W. J. Scheenen¹ · Arend Heerschap¹

Received: 31 December 2021 / Revised: 4 March 2022 / Accepted: 22 March 2022 / Published online: 20 April 2022
© The Author(s) 2022

Abstract

In this paper, we review the developments of ¹H-MR spectroscopic imaging (MRSI) methods designed to investigate prostate cancer, covering key aspects such as specific hardware, dedicated pulse sequences for data acquisition and data processing and quantification techniques. Emphasis is given to recent advancements in MRSI methodologies, as well as future developments, which can lead to overcome difficulties associated with commonly employed MRSI approaches applied in clinical routine. This includes the replacement of standard PRESS sequences for volume selection, which we identified as inadequate for clinical applications, by sLASER sequences and implementation of ¹H MRSI without water signal suppression. These may enable a new evaluation of the complementary role and significance of MRSI in prostate cancer management.

Keywords Prostate cancer · Proton magnetic resonance spectroscopy · State-of-the-art review · Spectroscopic imaging

Introduction

Prostate cancer (PCa) is the second most commonly occurring cancer in men and the fifth leading cause of cancer death, with an estimated 1.4 million new cases and 375,000 deaths worldwide in 2020. Relatively little is known about the etiology of PCa, however age, family history, and genetic mutations are established risk factors [1]. Since the 90's, prostate cancer mortality rates are declining in most countries with a high level of medical care [2, 3]. This is attributed to advancements in treatment and earlier detection through screening [4, 5]. In particular, prostate-specific antigen (PSA) testing allows early cancer detection and significantly affected mortality rates [6].

Autopsy studies of men not diagnosed with PCa have shown a PCa incidence of 60% in men over 80 years old [7], so screening for the disease with PSA testing also finds many cancers that would probably never need any treatment. Therefore, a major issue in PCa management is to distinguish between potentially aggressive cancers that are clinically significant requiring treatment and those that will not need immediate treatment [8]. In histopathology of biopsies,

the aggressiveness of tumor lesions is characterized by Gleason grades on a scale from 1 to 5, determined at two locations, which are combined in a Gleason score (GS). Often lesions with a $GS \leq 3+3$ are defined as low risk, with $3+4$ as intermediate and with $\geq 4+3$ as high risk. To better connect with clinical practice GSs are regrouped in Grade groups (GrG), i.e., $GrG1=GS \leq 6$, $GrG2=GS3+4$, $GrG3=GS4+3$, $GrG4=GS8$, $GrG5=GS9-10$ [9, 10].

The standard way to confirm the presence and nature of cancer in the prostate is transrectal ultrasound (TRUS)-guided biopsy specimens, analyzed by histopathology [8]. More recently, multi-parametric MRI (mpMRI) and MRI-guided targeted biopsy [11] have emerged as important tools in the detection, grading and staging of PCa [12–14]. The Prostate Imaging Reporting And Data System (PI-RADS) [13] aims at uniform reading of mpMRI in a structured reporting system assessing the likelihood of disease with clinical significance, using a combination of T2-weighted MRI (T2w-MRI), diffusion-weighted MRI (DWI) and dynamic contrast-enhanced MRI (DCE-MRI). In PI-RADS, the assessment by DCE is secondary to T2W and DWI. Recently, the necessity to use DCE is further disputed and using an endorectal coil at 3T is not advocated anymore [15]. In this way, the detection, localization, characterization, and risk stratification of tumors in patients suspected for PCa are improved [12, 16].

While MRI parameters can assess anatomical, morphological and some physiological abnormalities associated

✉ Angeliki Stamatelidou
Angeliki.Stamatelidou@radboudumc.nl

¹ Department of Medical Imaging (766), Radboud University Medical Center Nijmegen, Geert Grooteplein 10, P.O. Box 9101, 6500 HB Nijmegen, The Netherlands

with cancer development, complementary information on molecular aspects of this development can be derived from metabolic readouts, of which some may underlie earlier or more specific phases of disease progression. Tissue metabolites can be assessed non-invasively by ^1H Magnetic Resonance Spectroscopic Imaging (MRSI). In ^1H MRSI of prostate tissue a number of signals of metabolite protons, including those in citrate, choline compounds, spermine and creatine are detected. Ratios of these signals can serve as biomarkers in the detection, localization and characterization of PCa. As ^1H MRSI can be added, essentially seamlessly, to MRI procedures it may reinforce mpMRI in the non-invasive diagnosis of PCa [17–20]. In particular as mpMRI currently suffers from a low pooled specificity [21] and low inter-reader reproducibility [22].

Although MRSI was part of the first PI-RADS version, it was decided not to include it in later versions, i.e., PI-RADS 2.0 [23]. This decision was made because at that time the technique was less robust than the MRI methods and therefore difficult to apply successfully in clinical routine, in particular if no significant in-house expertise was available. Initially, it also required rather long examination times and lacked standardized automated processing and adequate data display [17]. Application of the technique is also muted by the still often encountered belief that an endorectal coil is an absolute requirement for MRSI of the prostate, while most MRI is now performed without such a coil.

Since its introduction, significant progress has been made in the development of prostate ^1H MRSI. This progress made it possible to acquire 3T MR spectra of voxels with effective sizes down to 0.3–0.6 cm³ with sufficient signal-to-noise (SNR) and spectroscopic resolution to detect metabolites of interest in measurement times below 10 min [17, 20].

MRSI of the prostate has been reviewed most recently by Tayari et al. [17], Kurhanewicz et al. [19], and Kobus et al. [24]. After these reviews some new developments concerning prostate MRSI with sLASER without an endorectal coil, prostate MRSI without water signal suppression and MRSI reconstruction have been presented. Furthermore, several new approaches improving MRSI of the brain have been reported that are promising for application to the prostate as well. For overviews including the application of other MRS methods to prostate cancer see Sharma et al. [25] and Jagannathan [26].

In this paper, we review recent developments of ^1H MRSI applied to prostate cancer, covering topics such as specific hardware, dedicated acquisition sequences and processing and quantification techniques. Emphasis will be given to advancements in MRSI methods that may overcome difficulties currently encountered in routine clinical MRSI applications, enabling a new evaluation of the complementary role and significance of MRSI for PCa management.

^1H MRSI of the prostate

Most clinical applications of MRSI employ the ^1H nucleus, because it is abundant in body compounds, has a relatively high sensitivity and the required MR hardware is widely available in the clinic.

^1H MR visible metabolites in the human prostate in vivo

The dominant metabolite peaks observed in MR spectra acquired from the prostate include those from protons in citrate, choline compounds, and (phospho-)creatine (Fig. 1). Usually signals of polyamines, mostly spermine, can also be detected [20, 27]. Furthermore, because of more recent progress in MRSI acquisition other signals, such as of myo-inositol and taurine, may be observed [28, 29] (Fig. 1). Since these signals and their ratios are used as biomarkers for prostate cancer or prostate abnormalities it is essential to understand their MR properties and biological context. Metabolite resonances in ^1H MR spectra of the prostate can be separated in those that arise from compounds dominant in the luminal ducts (citrate, myo-inositol, spermine) and those dominant in prostate cells (choline compounds, creatine).

Citrate (Cit) has two methylene groups with proton spins that are strongly coupled. Therefore it appears as a quartet signal in ^1H MR spectra with large variations in spectral appearances at different magnetic field strengths and pulse sequence timing [28, 30]. At lower field ($\leq 3\text{T}$), the two middle peaks dominate and resonate close together at about 2.6 ppm (Fig. 1). The citrate signal shape and chemical shift also depends on pH [31] and cation concentration [32].

The choline compounds glycerophosphocholine, phosphocholine and free choline (Cho or tCho for total choline) have nine chemically equivalent protons of three methyl groups resonating as a singlet around 3.19 ppm and two methylene groups, resulting in multiplets at 4.05 and 3.50 ppm. In practice, only the nine-proton singlet at ~ 3.19 ppm is evaluated because the intensity of the multiplets is very low in in-vivo MR spectra of the prostate.

Creatine (Cr) has five non-exchanging protons, a methyl group resonating at 3.03 ppm and a methylene group at 3.93 ppm. The protons in each group are chemically equivalent and uncoupled, resulting in two singlets [33].

Spermine (Spm) contains, next to its amine groups, ten methylene groups that form a weakly coupled spin system. The methylene protons consist of symmetrical pairs, giving a total of four protons resonating at about 1.81 ppm with further groups of four at about 2.11 ppm, 3.13

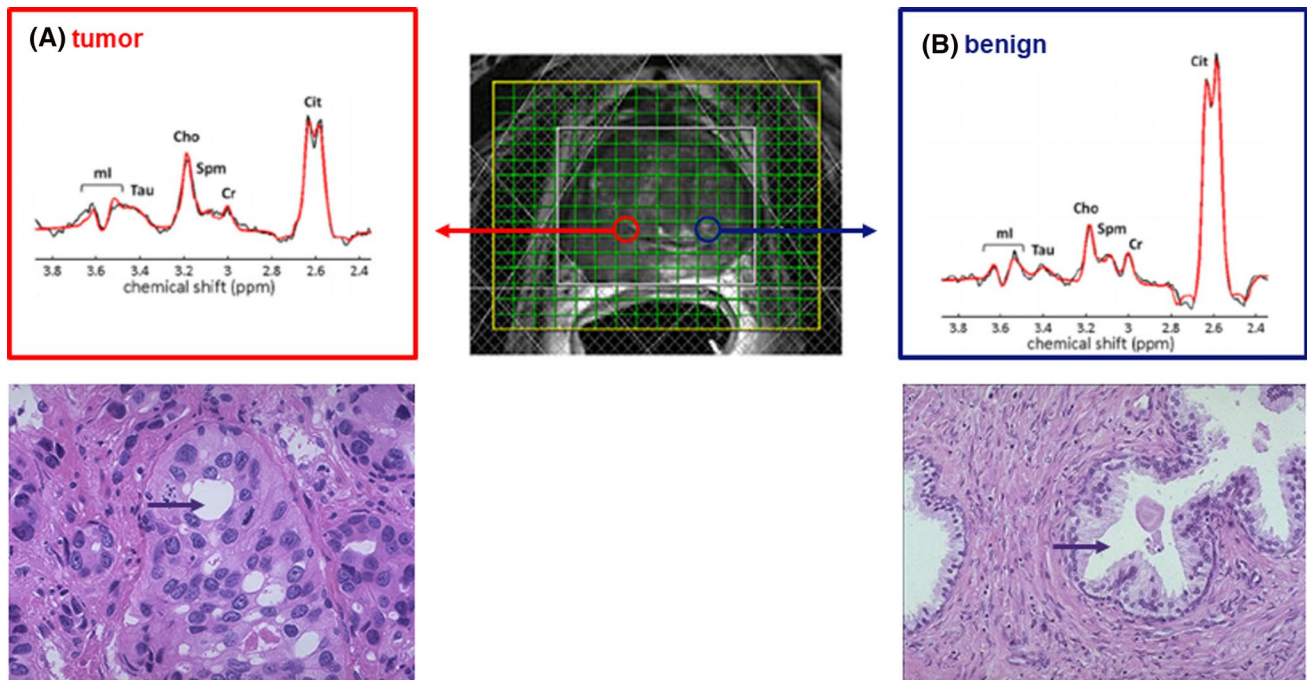


Fig. 1 3D MRSI of a patient with histopathology confirmed prostate cancer. The patient was measured at 3 T with an endorectal coil for signal reception and a GOIA-sLASER sequence for VOI (voxel of interest) selection of the prostate. The yellow box indicates the field of view and the white box the VOI. The hatched bars represent the OVS slabs. For further MR measurement details see [28]. On the T2w MR image with the MRSI voxel grid, the location of a tumor voxel (A) and a benign voxel (B) are indicated with circles to better represent their actual shape which is spherical due to the point

spread function. Representative MR spectra from tumor tissue and benign tissue are shown in panel A and B, respectively, illustrating decreased citrate and spermine and increased choline signals in the tumor lesion. Indicated are the signals for the prostate metabolites: citrate (Cit), choline (Cho), spermine (Spm), creatine (Cr), taurine (Tau) and myo-inositol (mI). Under the panels also histopathology slides are shown, illustrating the reduced luminal space in a cancer lesion in comparison with a healthy tissue (purple arrow)

ppm, 3.12 ppm, and 3.18 ppm. Usually only the signals at 3.12–3.18 ppm are evaluated as the others are suppressed due to lipid signal suppression pulses present in most pulse sequences. The chemical shift of these resonances is sensitive to pH and their shape and intensity may depend on TE [27, 34, 35].

Myo-inositol (mI) is a closed-ring sugar with six coupled protons resulting in a complicated spectroscopic shape with the highest intensity at about 3.5–3.6 ppm [36].

Metabolites in healthy prostate tissues

The healthy prostate accumulates high levels of Cit (Fig. 1b), in particular in the peripheral zone [37]. This zone consists of layers of glandular epithelial cells surrounding prostatic ducts. Epithelial cells in the prostate highly express the zinc transporter ZIP1 [38]. The resulting high intracellular concentration of zinc inhibits the enzyme aconitase in the tricarboxylic acid (TCA) cycle. This causes a high production of Cit at the cost of TCA cycle related energy production per molecule of glucose [36, 37]. The excess Cit is secreted in the prostatic fluid of the lumen and contributes to favorable

conditions for sperm maturation and motility in seminal fluid [41–43]. It has been reported that the Cit levels in normal prostatic fluid may vary considerably between about 10 and more than 300 mM [39, 40, 44, 45]. A mean value of about 100 mM is often assumed [44]. In vivo MRS assessments estimate normal prostate tissue Cit concentrations to be between 30 and 70 mM [29, 46–48]. With about a quarter of peripheral zone tissue volume occupied by ductal luminae this would correspond to Cit levels in prostatic fluid within these luminae between 120 and 280 mM. Similar tissue Cit levels were found in glandular prostate tissues by high-resolution magic angle spinning spectroscopy (HRMAS) [49]. In glandular tissues with benign prostatic hyperplasia (BPH), Cit levels may be higher [40, 47, 48], or lower in stromal BPH with less luminal space [49].

Myo-inositol is another major metabolite in prostatic fluid [45]. In this fluid, it occurs on average at about 6% of the citrate content which would mean that its normal tissue concentration would be 1–4 mM, although HRMAS studies estimate a higher tissue concentration [50]. The high concentration of myo-inositol in prostatic fluid serves multiple functions in male fertility such as in osmoregulation of

seminal fluid to enhance sperm motility and in improving sperm mitochondrial function [51].

In healthy prostate tissues, high concentrations of polyamines are present [49] mainly representing spermine [52]. Similar to citrate, they are secreted by specialized ductal cells in the prostate [53], and likewise accumulate in the luminal space [29]. Ornithine decarboxylase is the key, rate limiting, enzyme in the synthesis of polyamines. Apart from their role in proliferation and cell growth, they have various functions in fertility and contribute to the motility of sperm cells [54]. From extrapolation of prostatic fluid, HRMAS and in vivo MRS studies the tissue concentration of spermine is estimated to be 7–18 mM [29, 45, 49]. HRMAS studies indicate that the tissue content of polyamines are lower in stromal tissue and higher in glandular tissue [49]. A linear relationship between the concentration of polyamines (spermine) and citrate has been observed [36, 49, 55] and a transient association between citrate, spermine and zinc and binding of this complex to proteins has been deduced from in vitro T2 relaxation studies [56].

Choline and creatine compounds are present at relatively high concentrations in prostate cells. As these compounds are not detectable, or at very low concentrations, in prostatic fluid [36, 45], their signals observed in vivo must come from prostate tissue, which could be epithelial or stromal cells. From MRS measurements of healthy prostates the Cho tissue levels were estimated to be between 2 and 5 mM and those of Cr between 4 and 9 mM [17, 29, 33, 46, 49]. Creatine occurs at a higher level in stromal tissue, which is in agreement with the presence of smooth muscle in this tissue [57].

Healthy prostate regions, such as the peripheral zone, transition zone, areas next to the urethra, seminal vesicles and anterior fibromuscular stroma, may have different metabolite compositions. E.g., seminal fluid contains relatively high choline/glycerophosphocholine levels which may affect the spectra of voxels close to or overlapping the seminal vesicles [20, 58, 59]. In vivo ^{31}P MRSI measurements of the prostate identified phosphocholine rather than glycerophosphocholine as the main phospho-ester in seminal vesicles [60].

Metabolites in cancerous prostate tissues

In 1963, it was reported for the first time that citrate levels are decreased in prostate cancer tissue [61]. Later this was observed in vivo with ^{13}C MR spectroscopy [62], but it gained real interest as a potential diagnostic tool when it was demonstrated that this decrease could be detected with ^1H MR spectroscopy [63–67] (Fig. 1).

An early event in the development of cancer in the prostate is the downregulation of zinc transporters [38]. At lower zinc levels the inhibition of aconitase is released and

consequently TCA cycling is activated and citrate production and secretion is reduced. Glucose produces energy more efficiently, which may be relevant in malignancy and metastasis [68]. Next to reduced citrate secretion into the prostate lumen, cancer growth also causes a reduction in luminal space [69, 70]. Together these contribute to a lower citrate signal in ^1H MRSI voxels of cancerous tissue.

Together with a lower citrate signal, the intensity of polyamine (spermine) signals are decreased in ^1H MR spectra of cancerous prostate tissues (Fig. 1) [49, 50, 52, 55, 71]. This may similarly be explained by less spermine synthesis and decreased luminal space. Polyamine metabolism in prostate cancer is different from benign tissue and it may be relevant for disease progression that spermine can inhibit growth of PCa cells [72–74].

Abnormalities in the metabolism of myo-inositol have been documented and implicated in various disease states, including cancer [75]. In prostatic fluid of PCa patients, the concentration of myo-inositol is decreased [45].

Increased signals of lactate, commonly observed for tumors because of high glycolysis (i.e., Warburg effect), are seen in ^1H MR spectra of PCa tissue in vitro [49, 76], but these signals appear to be under the detection limit (~ 1.5 mM) of in vivo 3T MRSI of tumor lesions in the prostate recorded at TE = 144 ms [77]. Furthermore, the methyl lactate signal, if present, is easily obscured by signals of lipids resonating at a similar chemical shift or suppressed together with these signals, a common procedure embedded in most acquisition sequences.

In PCa tissues, the levels of choline compounds are increased, mainly due to a higher phosphocholine and glycerophosphocholine content [49]. This involves increased choline transport into tumour cells, increased choline kinase α and phospholipase A2 expression and activity in tumours [78, 79]. Rising choline levels in tumors are often associated with increased cell density and tumour hypoxia [80]. However, in prostate cancer tissue necrosis is rarely observed [9], which indicates that hypoxia, if present, is limited. In many MRS studies, a correlation has been observed between choline levels or choline signal ratios such as Cho/Cr or (Cho+Spm+Cr)/Cit and Gleason score [19, 71, 81–88]. The increased Cho/Cr ratio in high-grade tumors may also reflect decreased creatine, e.g., due to replacement of smooth muscle tissue by tumour cells or to changes in creatine metabolism [89].

Thus altogether, decreased levels of citrate, polyamines (i.e., spermine) and creatine and increased choline compound levels are attractive biomarkers to identify the presence of prostate cancer. However, some features of the prostate and its condition may mimic these changes and need attention in diagnosis. Citrate levels are highest in the normal peripheral zone and lower in areas close to the urethra. If BPH is mainly of stromal origin, this can result in relatively

low citrate levels [49]. As described above, seminal vesicles may contain high levels of choline compounds and need to be identified. Inflammation of the prostate, prostatitis, may mimic changes seen in prostate cancer. This ambiguity can be solved, since the Cit/Cho ratio appears to be higher in prostatitis than in tumours [90].

Hardware

Field strength

Common clinical MR systems employed for MR spectroscopy examinations have a field strength of 1.5T and 3T. Prostate MRSI at 3T can be performed at a higher SNR than at 1.5T, as illustrated by the two-fold increase in SNR for the inner citrate resonances, which enables MRSI with a higher spatial resolution [91]. Moving to 7T further increases SNR of prostate MRI 1.7- to 2.8-fold [92]. However, at this field it is more problematic to achieve sufficient RF power and field homogeneity in the prostate. These field-specific challenges are described in a separate paper in this issue [93]. At higher spatial resolution, the MRSI matrices to cover the whole prostate increase, which requires more repetitions in traditional 3D phase encode sampling and therefore may result in too long acquisition times for clinical exams, requiring accelerated acquisitions, e.g., with spiral readouts [94–96].

Endorectal or phased array RF coils

MRSI of the prostate commonly involves spin excitation with a body coil and signal reception with an external multi-channel phased array and/or an endorectal coil (Fig. 2) to receive the MR signal [17, 35, 97]. At 1.5T the use of an endorectal coil (ERC) is recommended if spatial

resolutions below 1 cm^3 are desired with sufficient spectroscopic SNR [20, 98, 99]. Endorectal coils are available in several versions requiring different operating procedures, each with specific benefits and disadvantages for MRS exams [100–105]. Although SNR is lower with phased array coils at 1.5T their use still may have diagnostic value [104].

At 3T MRSI can be performed without an ERC [106], but its use still improves cancer localization compared to using only external phased-array coils [107]. However, a comparison of PCa diagnosis by MRI at 1.5T with ERC and 3T without indicated a similar performance in cancer detection [108]. Although an ERC provides high SNR, especially near the coil, which can be exploited to reduce measurement time or to increase spatial resolution [83, 109] it has several disadvantages in clinical routine compared to phased array coils. For instance, an ERC is costly, its positioning is time consuming, requires experience, is uncomfortable for patients, is associated with signal drop in the coil FOV and causes artefacts [15]. Moreover, using an ERC reduces the SAR limit set by the MR system, which leads to longer acquisition times. Therefore, mpMRI of the prostate is now mostly applied at 3T without ERC, i.e., with external body phased array coils and hence it is relevant to demonstrate that clinical 3D MRSI of the prostate can also be performed without ERC at 3T [81, 88]. Using PRESS for acquisition, the quality of MRSI at 1.5 T with ERC is comparable to that at 3T without ERC, except for voxels located close to this coil, which have a higher SNR [110]. The loss in SNR by performing MRSI at 3T with a phased array coil combination instead of an ERC can be mitigated using LASER type of acquisition sequences [17, 28, 96]. Several studies have demonstrated that in this way MRSI of the prostate can be performed reliably within acceptable time in clinical routine [28, 82, 106, 111].

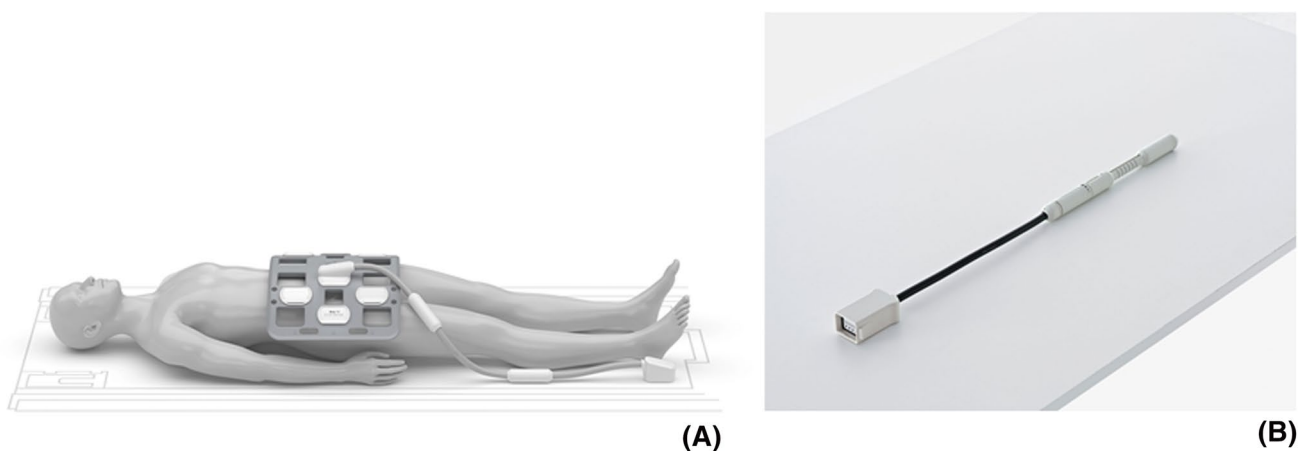


Fig. 2 Coils for MR signal reception used for prostate 1H MRI and MRSI. **A** External phased array coil positioned on a patient for prostate MR examinations [233]. **B** Endorectal surface coil for positioning in the rectum [233]

Acquisition

Shimming

An essential first step towards the acquisition of high-quality ^1H MRSI data is optimization of B_0 field homogeneity (shimming). This strongly affects spectral quality, since inhomogeneous fields broaden the spectroscopic signals due to faster decay of the apparent transverse magnetization in a voxel. If this causes overlap of signals, it can affect the reliability of their quantification. This may be a challenge for the signals of choline, spermine and creatine, which resonate rather close to each other. Good B_0 homogeneity is also crucial for effective water and lipid signal suppression, since when the signals are broadened or shifted they may escape the frequency-selective pulses needed for their suppression [20]. The signal broadening effects of field inhomogeneity may be restored by a modulus operation on the FID of water signal unsuppressed ^1H MRSI [88, 112–114]. A recent post-processing approach to restore field inhomogeneity effects in prostate MRSI is over-discretized reconstruction, which appears to improve lipid signal contamination [115]. Finally, a practical step to improve the B_0 inhomogeneity is the preparation of the rectum with a cleansing enema and an endorectal gel filling [116].

Pulse sequences

Initially, localized in vivo MR spectra of the human prostate were obtained using only the field of view of an endorectal coil and single voxel MRS [33, 62, 97]. Volume localization of the prostate for ^1H MRS was first performed with stimulated echo acquisition mode (STEAM) and point-resolved

spectroscopy (PRESS) sequences [117, 118], of which the latter is commonly applied in the clinic (Fig. 3a). Because of the multi-focal and heterogeneous nature of prostate cancer these volume selection methods are now mostly employed in combination with 3D MR spectroscopic imaging methods to cover the whole prostate [19, 20, 119].

More recently, adiabatic pulses were introduced for volume of interest (VOI) localization by adiabatic selective refocusing (LASER) sequences, in which paired adiabatic refocusing pulses are applied for slice selection of a VOI. In the most popular version one pair is replaced by a standard 90° excitation pulse, which is called semi-LASER [28] (Fig. 3b). Adiabatic pulses have better slice profiles, reducing outer volume signal contamination and are less sensitive to RF transmit field inhomogeneities [120, 121]. Also, they have a wide excitation bandwidth, which reduces the chemical shift displacement artefact (CSDA) [122]. However, they are RF power-demanding and need to be applied in pairs to achieve a homogeneous phase distribution over the selected slice, which limits their use [123]. To lower RF power deposition, gradient-modulated offset independent adiabaticity (GOIA) pulses [124] have been implemented for prostate MRSI, since they require less RF power to reach adiabaticity [24]. The application of GOIA-sLASER to prostate MRSI considerably reduces the contamination of spectra with lipid signals of fat surrounding the prostate and hence improves the quality of the spectra and robustness of the measurement [28]. As the T1 relaxation times of the proton spins in prostate metabolites are relatively short (compared to those in the brain), it is possible to select rather short repetition times (TR) so that for instance in a $12 \times 12 \times 10$ matrix in 3D MRSI with GOIA-sLASER, the measurement time can be reduced to less than 7 min without an endorectal coil with a nominal voxel resolution of $7 \times 7 \times 7$ mm [81].

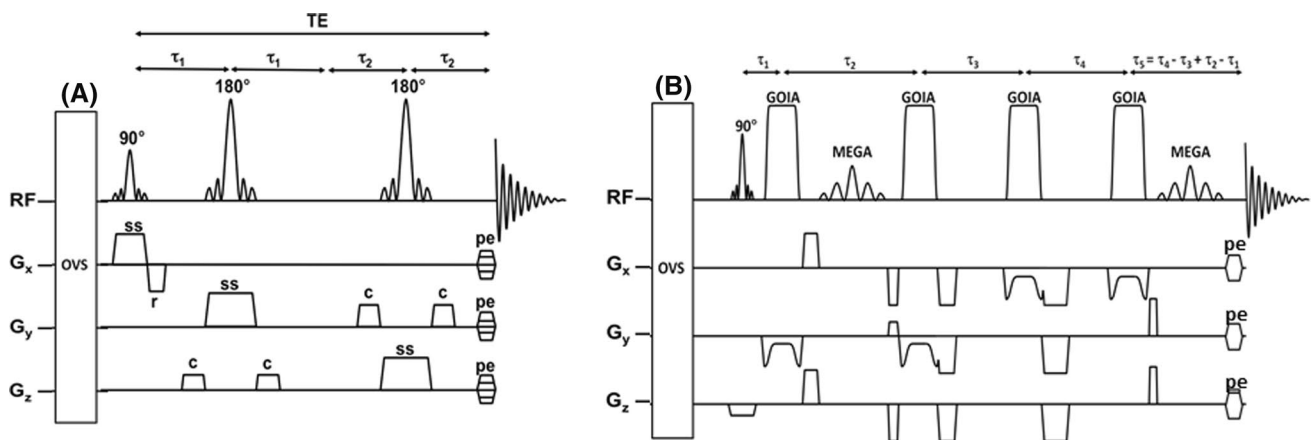


Fig. 3 MRS pulse sequences used for volume selection of the prostate. **A** PRESS (point resolved spectroscopy) pulse sequence. OVS=slice selection for outer volume suppression. MEGA: frequency selective pulses for Mescher-Garwood spectroscopic sup-

pression. Acq: acquisition. Interpulse timings are indicated [17]. **B** sLASER pulse sequence. After excitation with a conventional slice selective excitation pulse, the signal is refocused with two pairs of slice-selective low-power adiabatic GOIA refocusing pulses [17]

To speed up the measurements in Cartesian k-space sampling for MRSI, it is common to apply weighted sampling and Hamming k-space filtering. This also reduces spatial side bands from the point spread function, but enlarges the true voxel sizes [28, 96]. To still keep the intended voxel size within limits, larger sampling matrices and field of views (FOV) can be selected, which however may considerably increase measurement times in the case of large prostates. Therefore, to be more flexible, it is advantage to use rapid k-space sampling schemes such as in EPSI or spiral SI acquisition [96, 119, 125].

Also sequences with spectral–spatial-selective pulses were developed that fully excite metabolite spins in the prostate, but not those of peri-prostatic lipids and water [91, 126]. These sequences successfully have been applied in prostate MRSI at 1.5T, 3T and 7T [35, 91, 126], but are sensitive to B_0 inhomogeneities.

Although MR spectra of the prostate can be acquired by MRSI with fairly resolved signals of metabolites (see Fig. 1) often there is more overlap, in particular between Cho, Spm and Cr and with lipid signals. Therefore, specially designed pulse sequences have been developed to selectively detect Spm or Cit signals [127, 128]. Separation of signals in complete MR spectra of the prostate can be enhanced by J-resolved and correlated spectroscopy which disperses the overlapping resonances into a second dimension, reducing congestion and increasing metabolite specificity, such as for Cho, Spm and Cr and in the detection of glutamate/glutamine and other resonances [129–133]. As these two-dimensional methods are time consuming their MRSI localized versions became too long for clinical applications. This problem was solved by employing readouts with EPSI and compressed sensing (CS), in which signals can be recovered from an acquisition that uses fewer samples than required by Nyquist–Shannon [134, 135]. Currently, for the prostate, these technically advanced methods still have only been applied to human prostate in 2D MRSI mode with relatively large voxel sizes.

Echo time selection

For spin-echo type localization sequences commonly the shortest possible echo time (TE) is selected to acquire as much signal as possible minimizing T2 relaxation losses. However, in most prostate MRS(I) experiments, a longer TE is chosen to decrease nuisance signals such as of lipids. The signal of the strongly coupled spin system of citrate is dominating in prostate MR spectra and shows considerable variations as a function of interpulse timing (including TE). Therefore, for each pulse sequence timing and field strength a TE is selected with a high citrate absorption signal intensity [30, 136–139]. Typical TE's for PRESS volume selection at 1.5T are 120–130 ms, at 3T 85–145 ms [140] and at

7T 71–142 ms [35]. For semi-LASER, at 3T an optimal TE of about 85 ms was selected [28] and at 7T of 56 ms [141]. However, successful 2D MRSI of the prostate with TE's as short as about 30 ms has been performed [29, 142].

Movement artifacts

Prostate MR measurements may suffer from movement artifacts, due to the location of the prostate near the bowels and relatively long acquisition times. In patients several approaches are available to minimize these artifacts. To limit bowel movement preparation techniques can be performed, including the use of anti-peristaltic drugs, e.g., glucagon or butylscopolamine bromide and the application of micro-enema to evacuate the rectum if necessary. Dietary restrictions, where the patients are instructed to fast 6h prior to the exam and consume water solely, even though widely applied, do not appear to provide a significant benefit in data acquisition [143]. However, no study specifically addressing the value of bowel preparation in prostate MRSI has been reported. Potential acquisition techniques to reduce motion artifacts include the application of a navigator [144] or to apply rapid acquisition methods, such as spiral readouts starting at the center of the k-space to correct for motion induced phase variations [96, 145]. Finally, in water signal unsuppressed MRSI the water signal can be used to mitigate movement artefacts [112].

Lipids and water signal suppression

As the prostate is embedded in lipid tissue substantial contamination by lipid signals may occur in MR spectra of prostate voxels, close to the resonances of interest (i.e., of citrate), for instance if the selected VOI overlaps with lipid tissue, by B_0 inhomogeneity or by bad VOI selection causing signal bleeding from “lipid” voxels at the VOI edges to other voxels by the point spread function. Pulse sequences with bad VOI selection are a main reason for low quality MRSI data and ultimately hamper the correct quantification of metabolite signals. To prevent lipid signal contamination in prostate spectra several techniques have been used, including outer volume saturation (OVS), additional pulses for lipid and water signal suppression, spectral–spatial-selective pulses, better VOI selection (see section “Pulse sequences”), k-space apodization [17], the use of FID modulus [112, 113] and over-discretized reconstruction [115].

It is common to apply outer volume saturation (OVS) bands, positioned around the prostate to reduce extraprostatic lipid signals (Fig. 1). All spins in these bands are excited and then dephased by crusher gradients. OVS pulses were developed to compensate for poor edge profiles, B_1 field inhomogeneity and chemical shift errors, such as very selective saturation (VSS) pulses with reduced B_1 and T_1

dependency [146]. The OVS slabs are usually placed manually, which is subjective and time-consuming, and limits the number of slabs to be placed. Therefore, automated algorithms have been developed, to optimize orientation, timing and flip angle setting of the VSS pulses following the shape of the prostate [147, 148]. Also, supervised 3D fully convolutional networks have been developed, for automatic prostate MRI segmentation [149], that can be extended to MRSI. As OVS selection may affect spectra of voxels at the edge of the prostate it is recommended to keep the number of slabs low and rely on the proper implementation of other options for lipid signal suppression (see above).

A widely applied approach is spectroscopic signal suppression with double band-selective inversion with gradient dephasing (BASING) [150, 151] or Mescher–Garwood (MEGA) [152], in which dual-frequency pulses surrounded by crusher gradients, selectively invert and dephase both the lipid and water signals.

Signal contamination between neighboring voxels, due to the side-lobes of the spatial response function (SRF) can be significant when peri-prostatic areas with high lipids are included in the VOI. These side-bands are commonly attenuated with a Hamming apodization filter in k-space [153]. Combined with weighted elliptical k-space sampling this results in a considerably shorter acquisition time [154], which however increases voxel size, and thus SNR, but reduces spatial resolution [96, 155]. Another significant method to prevent lipid contamination is the application of more accurate localization sequences (see above Pulse sequences [77, 156]).

Processing and interpretation of ^1H MRSI data

Current protocols to process MRSI data require the performance of multiple steps, like quality control of spectra, localization of cancer suspicious voxels with reference to MR images [86, 138, 157], and judging a spectrum as ‘suspicious of tumour’ or not [158, 159]. Proceeding through all these steps manually is time consuming and requires significant effort, since thousands of spectra are acquired from each patient, which demands time and experience of the users. Therefore, automation in data processing is essential in clinical routine.

The following paragraphs discuss processing steps for ^1H MRSI data of the prostate and how these steps can be performed in a reproducible, automatic way.

Signal preparation

In case of data acquisition with multiple receive coils, the signals of these coils have to be properly combined and

arranged in k-space, which may require specific methods for MRSI applications [160]. In case of signal reception with an endorectal coil B1 inhomogeneity may have to be corrected [161]. For MRSI usually apodization filters are applied, to improve the shape of the SRF, and the matrix of the data is zero filled, to facilitate a better localization of spectra, but causing smaller voxel sizes than the acquired true voxel size.

Phase and frequency corrections

After Fourier transformation signal frequency and phase errors may have to be corrected. Numerous algorithms exist for automated phasing and frequency alignment, e.g., [162–164]. Phase correction may be avoided by working on magnitude spectra, but this broadens the line width, reducing spectroscopic resolution. If water signal unsuppressed data are acquired an automatic way for phase and frequency alignment is by computing the modulus of the time-domain MRS signal [113, 165]. Furthermore, principal component analysis can be used to calculate phase and frequency deviations and correct them to achieve an iterative improvement in similarity across all spectra [166, 167]. This has been adapted to automatically correct ^1H MRSI data of patients with prostate cancer [163].

Baseline correction

In MR spectra, a baseline can be present under the metabolite signals due to broad signals of macromolecules, insufficient suppression of water and lipid signals or first order phase roll. This baseline has to be taken into account for a proper quantification of metabolite signals. As most prostate MR spectra are acquired with spin-echo type of pulse sequences, acquisition can start at the center of the echo, minimizing first-order phase errors. Fortunately, in contrast to MR spectra of the brain, there is no significant contribution of macromolecular signals to the baseline in MR spectra of the prostate down to echo times of 32 ms [18, 29]. Baseline corrections may be needed if the tails of broad water or lipid signals stretch out into the spectral region of interest (about 2.3–4 ppm). These contaminating signals occur less often with adiabatic volume selection such as applied in sLASER than with PRESS using standard refocusing pulses [28] and are also attenuated at $\text{TE}'\text{s} > 100$ ms.

Most quantification software includes a baseline component within the FID or spectrum model. This baseline is often assumed to be a smoothly varying line that can be modelled with splines [168–170] or estimated by smoothing the spectrum [157, 171, 172]. The baseline is corrected together with metabolite fitting by iterative optimisation. Baseline correction without any metabolite estimation is suitable for pattern recognition analysis. This can be achieved by filtering firstly water and lipid signals [173,

[174], or by fitting a lipid peak to the spectrum and subtracting it from the region of overlap with the citrate resonance [164]. Accurate baseline correction is important if signal integration is used for quantification. This may require additional quality control as even small variations from zero at the base of a metabolite peak can generate large errors in its total area estimate [138, 175].

Lineshape modelling and linewidth

Field inhomogeneities within ^1H MRSI voxels, eddy currents and bad shimming result in non-Lorentzian lineshapes with variable line widths. In quantification algorithms a variable to describe this lineshape can be included, assumed to be the same for each peak within one spectrum, or it can use a fixed model shape, like Gaussian, allowing some variation of the linewidth [86, 176, 177]. Numeric integration can be affected negatively by changes in linewidth if the width of the chemical shift region for integration is fixed [150]. An increased linewidth leads to less of the peak within the integration window and an artefactual underestimation of the resonance area. The effects of varying linewidth need to be checked in a quality control step prior to integration of metabolite quantities or, alternatively, linewidths can be adapted according to the quality of each voxel shim [178].

Spectroscopic quality control

As SNR in MRSI is limited the technique is prone to artefacts and therefore spectroscopic quality control is an essential step in the clinical pipeline. Quality control can be performed qualitatively by experts, but this is time consuming and not objective. Therefore, automated methods have been developed. In one method, a nonlinear classifier of magnitude spectra was used to determine whether spectra were of suitable quality [174]. The classifier was trained on data that expert spectroscopists had graded to be of acceptable or unacceptable quality. Another approach applied feature extraction of the real part of the spectra to reduce it to a small number of scores [179]. The feature extraction is a linear fit of components generated by independent component analysis of spectra from a training set of similarly acquired ^1H MRSI data. A nonlinear classifier was then applied to these scores rather than the full spectra. The quality control of the spectra was implemented with feature extraction of test-set spectra. Finally, a simple spectroscopic quality control of prostate MR spectra has been proposed in which a ratio of components contributing to bad spectra (noise, lipid signals) and those contributing to good quality spectra (Cit, Cho signals) is used as an index to exclude bad quality prostate MR spectra [180].

Applying a set of rules to judge spectroscopic quality in 3D MRSI of patients by an expert panel showed that using

a PRESS volume selection sequence at 1.5T resulted in 33% of voxels with bad quality spectra, while this number was 17% for PRESS applied at 3T and 11% for sLASER applied at 3T without using an endorectal coil. This indicates that PRESS 3D MRSI applied at 1.5T was not well suited for clinical routine, in contrast to the currently used sLASER 3D MRSI [179, 180].

Spectroscopic evaluation

Metabolite signals in prostate MR spectra can be evaluated qualitatively, for instance, by visually inspecting signal intensity decreases of Cit and Spm and a signal increase of Cho as spectroscopic signatures to identify cancer lesions. However, as this is subjective it is preferred to employ quantitative methods, for instance by peak fitting, either in time or frequency domain. Most MR systems have software to determine peak areas, but it is also possible to export MRS data to specialized spectroscopic processing packages, such as LCModel [170, 181], jMRUI [182, 183] and Tarquin [184]. Because of the use of endorectal coils with an inhomogeneous receive B_1 field by which signal intensity of the coil drops towards the ventral parts of the prostate, it has become custom to calculate signal ratios, avoiding intrinsic spatial variations in signal intensity. Because it is not always feasible to resolve Cho from Cr and Spm signals, in particular at 1.5T and with PRESS sequences, the most often used ratios are (Cho+Cr)/Cit and (Cho+Spm +Cr)/Cit [18]. With better resolution, e.g., at 3T, it is common to also use Cho/Cr [81] and Cho/Cit ratios. For the localization and characterization of cancer lesions, threshold values for these ratios are determined and ratio maps constructed (Fig. 4c). With phased array coils, which have a homogeneous B_1 receive field within the prostate, it is possible to evaluate and map the signals of individual metabolites [81].

Absolute tissue concentrations of metabolites (Abs_{con}) can be obtained using the signal of internal water as a reference. As this requires an additional time consuming MRSI measurement without water signal suppression, it is not commonly applied [33, 47]. However, we recently demonstrated that with water signal unsuppressed MRSI of the prostate it is possible to use the intravoxel water signal as a reference to obtain Abs_{con} values. This signal was extracted from the spectra either with water-signal modeling [185] or with tensor-based Blind Source Separation [114].

Abs_{con} is derived from the metabolite signal relative to that of water (S_{rel}), applying correction factors for T_1 and T_2 relaxation of both metabolite (T_{1met} , T_{2met}) and water reference (T_{1ref} , T_{2ref}) according to Equation 1. Relevant T_1 and T_2 relaxation times for prostate compounds are presented in Table 1. Abs_{con} is then calculated from the water concentration of prostate tissue $wcon=40.2$ mM, assuming a

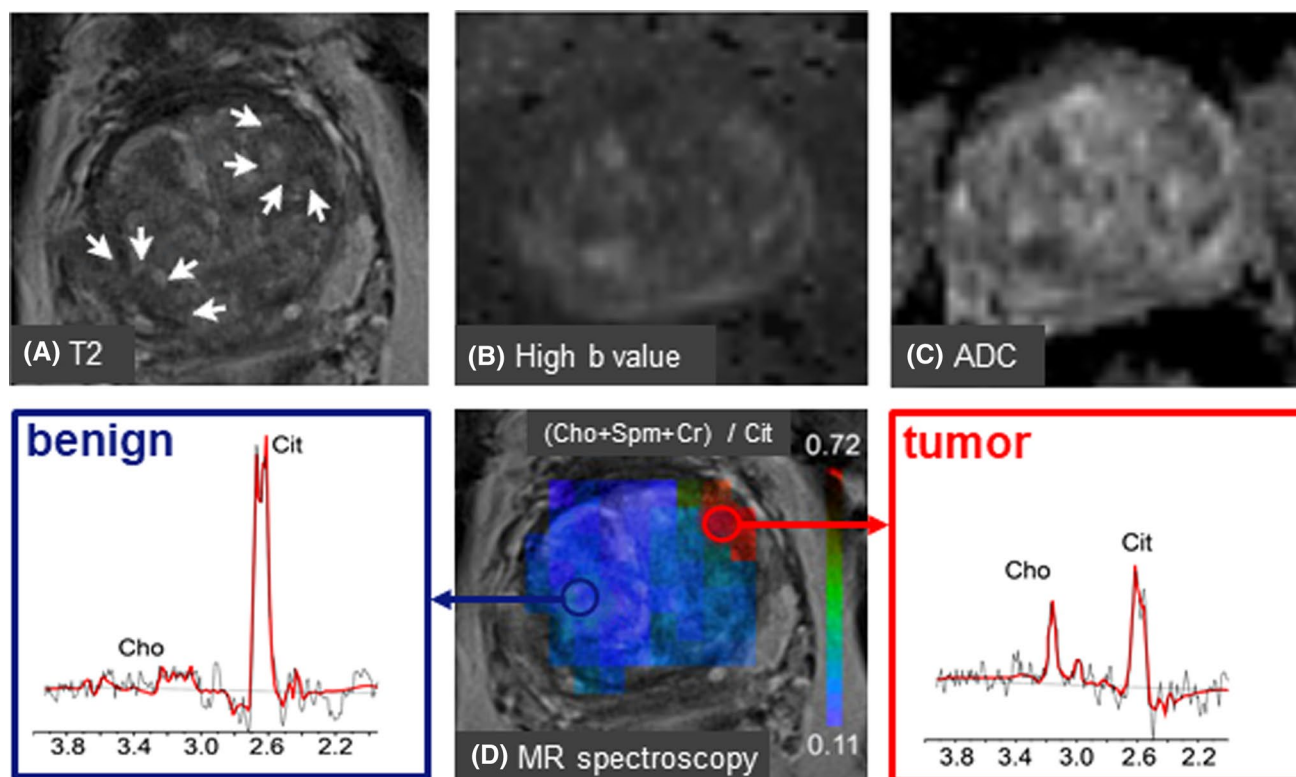


Fig. 4 3D MRSI identifies correct tumor lesion after ambiguous T2 and DWI MRI in the mpMRI examination of a patient with serum PSA of 4.3 ng/ml. The MR investigations were performed at 3 T with a phased array coil for signal reception. For details see [111]. **A** Transversal T2 w MRI shows at least two locations with low signal intensity suspicious for cancer in the left and right side of the transition zone (TZ) of the prostate (white arrows). **B** Both these locations have high intensities in high b value maps suggesting the presence of tumor tissue. **C** This assignment seems to be confirmed by ADC

maps with low intensities at both positions. **D** A metabolite ratio map obtained from 3D MRSI with a GOIA-sLASER sequence shows a hot spot for only the left TZ location. An MR spectrum obtained from this location shows a low citrate and increased choline signal compared to the right TZ location. This identifies the left TZ lesion as cancer tissue and the right TZ lesion as benign. This was confirmed by histopathology of biopsies from both locations, which identified the left TZ location as a low-risk cancer lesion and the right TZ location as benign. *Cho* choline; *Cit* citrate

Table 1 In-vivo T1 and T2 relaxation times of the prostate metabolites of interest

Metabolite	T ₁ (s)	T ₂ (s)
1.5 T Citrate [33, 47]	0.34 ± 0.04	0.17 ± 0.02 (PZ) 0.12 ± 0.03 (TZ)
Choline [33]	0.84 ± 0.09	0.23 ± 0.06
Creatine [33]	0.86 ± 0.1	0.21 ± 0.1
3 T Citrate [30]	0.47 ± 0.14	0.17 ± 0.05
Choline [30]	1.1 ± 0.4	0.22 ± 0.09
Creatine [46]	1.13 ± 0.15	0.19 ± 0.02
Spermine [29]		0.053 ± 0.016
Myo-inositol [29]		0.090 ± 0.048
Water-healthy tissue(PZ)	1.756 [234]	0.142 ± 0.024[235]
Water- cancer tissue(PZ)	1.301 [234]	0.109 ± 0.020[235]

prostate tissue water content of 39.4 mM/ gr wet weight and a tissue density of 1.02 kg/l [47, 186].

$$Abs_{con} = Srel \frac{\left[1 - e\left(-\frac{TR}{T_{1,ref}}\right) \right] \left[e\left(-\frac{TE}{T_{2,ref}}\right) \right]}{\left[1 - e\left(-\frac{TR}{T_{1,met}}\right) \right] \left[e\left(-\frac{TE}{T_{2,met}}\right) \right]} wcon \quad (1)$$

In the calculations for prostates with cancer lesions, it was assumed that T1 and T2 values of metabolite spins and $wcon$ do not differ between tumor and cancer tissue, while different relaxation values for water spins were implemented (Table 1). Indeed, it is known that tissue water content is rather homogenous over the prostate and does not differ between tumor and benign tissue. Because both T2 and T1 values of water spins in tumors decrease the relaxation correction factor for these spins in benign and tumor tissue are similar for common Tr values, implying that spatial maps of

Abs_con obtained with this correction factor directly reflect differences in metabolite content between tumor and benign tissue [185].

Pattern recognition

An alternative quantitative approach to distinguish tumour from benign tissue is by pattern recognition. The process is based on feature extraction, reducing the dimensionality of the MRS data so that useful information is retained, while irrelevant components and noise are removed. Then, these features are classified, separating the data into the anticipated groups. In pattern recognition, spectra are classified without using a biological model and are trained on feature-extracted data to establish which features are important for discrimination. Thus, maps of tumour presence or aggressiveness can be created from the raw data. For instance, it was reported that using nonlinear classifiers on feature extracted data can better separate malignant from benign prostate tissue than using quantification algorithms [187]. Also, a partial least squares regression approach of magnitude spectra achieved similar classifications of benign and tumorous tissues as experts [174].

¹H MRSI in clinical applications

In clinical applications, 3D ¹H MRSI of the prostate is always applied within a mpMRI approach including T2 weighted MRI and DWI and often DCE MRI so that anatomical and other functional information is also available [12]. Within this context, MRSI has been demonstrated to have significant clinical value in most steps towards PCa diagnostics, including in-vivo detection and localization of tumor lesions, tumor staging, determination of tumour aggressiveness and therapeutic planning and evaluation [19, 20, 86, 157, 188, 189].

Detection and localization of prostate cancer lesions

For patients with clinical signs suspicious for the presence of PCa the performance of a mpMRI exam is recommended to detect if significant cancer is present. This exam is also important to identify the locations of cancer lesions in the prostate as this information is relevant for staging, TRUS- or MR-guided biopsies, preparation of a radical prostatectomy and guidance for focal therapies [12]. The ability of ¹H MRSI to detect and localize cancer tissue in the prostate has been demonstrated by numerous studies [17, 19, 20], including multi-center trials [87, 138].

Several studies showed that the sensitivity of ¹H MRSI to identify cancer lesions increases with the GS, for instance at 1.5T a sensitivity increase from 44 for 3 + 3 to 89% for \geq

4 + 4 GS lesions was recorded [157] and the sensitivity for the detection of high-grade was greater than of low grade disease ((92.7 vs. 67.6%) [190]. Most likely the smaller volume of the low-grade lesions contributed to this lower detection sensitivity by ¹H MRSI at 1.5T due to a partial volume effect involving signal mixing with normal prostate tissue in the voxels. However, the better sensitivity in detecting high-grade tumors might be used to exclude patients with these tumors from active surveillance [190].

In a prospective multi-site study, it also appeared to be difficult to detect low grade, small volume tumors [159]. Together with a low overall spectroscopic quality in this and other studies this raised questions about the role of MRSI in detection of tumors in clinical routine [191]. However, most clinical studies until recently were performed with standard PRESS localization at 1.5T with endorectal coil or with standard PRESS at 3T without endorectal coil. As outlined above our quality assessment demonstrated that a substantial fraction of MR spectra measured by MRSI under these conditions have insufficient quality and hence are not suitable for routine clinical applications (see above).

As also outlined above the robustness of MRSI can be improved using LASER type of sequences. In recent studies, it was demonstrated that employing a GOIA-sLASER sequence at TE=88 ms and only a phase array coil for acquisition and using a support vector machine model analyzing several metabolite ratios, it is possible to discriminate tumor lesions, of low up to high GS, from normal prostate tissue in the transition zone with high accuracies of 96% [82]. Even better results were obtained in an mpMRI exam, in which MRSI was combined with T2 weighted and diffusion weighted MRI [111]. The complementary role of MRSI in tumor localization by mpMRI is illustrated by the case shown in Fig. 4, in which ambiguity about the tumor location after T2 and DWI MRI could be solved by adding MRSI data. Similar results on the value of MRSI in the separation of tumor lesions and normal prostate tissue by mpMRI were reported for examinations performed with an endorectal coil at 3T using an MLEV-PRESS sequence for volume selection at TE=85 ms [83].

Tumor aggressiveness

Because most prostate cancers grow slowly and are not life threatening it is a major clinical problem to identify aggressive tumors among indolent ones to avoid overtreatment. Low aggressive tumors may be selected for active surveillance instead of surgery or another drastic treatment. For instance a clinically non-significant tumor nodule is organ-confined with no GS higher than 3 and with a volume smaller than 1.3 cm³ [192]. As Gleason scoring from biopsies suffers from sampling errors it would be very important if functional imaging could discriminate between aggressive

and indolent tumors and predict progression of the latter to aggressive variants.

In general, a correlation is found between GS and metabolite ratios, but the overlap of ratio values between risk groups precluded to only use these to assign individual cases to certain risk groups, although MRSI appears to perform better than DWI in the transition zone, while DWI performs better in the peripheral zone [193]. However, in some studies reasonable separations between low risk and higher risk cancer lesions were obtained when metabolite ratios were combined with T2 w MRI, DWI or DCE parameter values [194]. By adding MRI and MRSI measures to a clinical nomogram, it was possible to identify significant cancer at an AUC of 0.85 [195]. In a study using a GOIA-sLASER sequence at 3T with TE=88ms to measure metabolites and a support vector machine analysis it was possible to separate low risk cancer lesions from high risk in the transition zone in a combination of ADC, Ktrans and metabolite ratios at an AUC of 0.86, while AUC was only 0.64 if ADC was combined with Ktrans [111].

Challenges and future directions

Although mpMRI is widely applied to men with elevated PSA to detect clinically significant PCa a recent Cochrane meta-analysis revealed that the pooled specificity of mpMRI was only 37%, despite a high sensitivity [22]. Moreover, mpMRI suffers from low inter-reader reproducibility [21, 22]. This clearly indicates that additional approaches are needed to improve PCa diagnosis. Currently, the role of DCE MRI as a useful part of an mpMRI exam is under discussion because of the relatively small contribution to diagnosis and time and effort to prepare the patient for iv injection and costs [196, 197]. For these reasons, the inclusion of ^1H MRSI in mpMRI may be considered as a valid alternative, even if only selected to assist in equivocal cases. For MRSI to be included in routine clinical workflow, some of the innovations described in this review are indispensable and still further innovations would be helpful to improve robustness, speed, spatial resolution and data processing. Some recent new technological developments are anticipated to provide these improvements for clinical prostate MRSI.

As described above the replacement of standard PRESS volume selection by sLASER is a major step forward and MRSI with sLASER in a mpMRI approach using machine learning yielded excellent results in the detection and localization of cancer lesions in the prostate and determination of the aggressiveness of the disease [111]. Another potentially important new acquisition option is sLASER volume selection in MRSI without water signal suppression. This may open new opportunities in the diagnostics of prostate diseases as it simultaneously provides information of both

water and metabolite signals. Moreover, the water signal can be used to correct for line shape artefacts, as a reference to estimate absolute metabolite levels, and to accurately combine signals of multiple coil elements with different sensitivity profiles. We recently demonstrated for water-unsuppressed MRSI of the prostate that it is possible to remove the water signal and its artefacts in postprocessing and use this signal for referencing purposes [88]. Because no additional MRSI acquisition is required it can be performed within a clinical exam [88, 114].

New options for accelerated 3D MRSI acquisition of the brain, such as by SPICE (SPectroscopic Imaging by exploiting spatiospectral CorrElation), which makes high-resolution metabolic imaging possible by incorporating prior information and field inhomogeneity corrections, or by compressed sensing and low rank reconstruction, may be of interest for prostate applications as well [198–200].

In the recent past, the use of an endorectal coil was considered inevitable for MRI and MRS of the prostate to obtain data with sufficient SNR and spatial resolution. However, upon increasing field strength from 1.5 to 3 T it has become common to perform MRI without an ERC as it turned out that clinical performance was similar, patient discomfort is relieved, patient preparation time is shortened and avoids the cost of an ERC. Therefore, it is unavoidable that clinical MRS of the prostate also needs to be performed without an ERC, even though it has been advocated that detection of small lesions may require such a coil [83]. In several studies, it was shown that MRSI of the prostate with a phased array coil is feasible at 3T, moreover the application of an sLASER sequence at a TE of about 85 ms substantially improved SNR allowing to perform MRSI of the prostate with a high reliability [28, 201].

Local B_0 field inhomogeneities, caused by magnetic susceptibility differences between prostate tissues, may affect MRSI quality. The most severe inhomogeneity occurs at air-tissue transitions such as at the rectum. Commercial MR systems can correct for B_0 inhomogeneities with shim coils, but these usually are not able to handle multiple boundaries with strong susceptibility transitions [18]. To improve this situation, a range of dedicated technical solutions have been developed, mostly for brain applications [202–206]. It would be of great interest to explore some of these for prostate applications in particular as diffusion MRI of the prostate, the mainstay in PCa diagnosis, also suffers from problems with susceptibility transitions. Local B_0 inhomogeneities can also be corrected in postprocessing such as by over-discretized reconstruction, which was demonstrated to improve signal localization in prostate ^1H MRSI, and therefore reduced lipid signal contamination [115].

Currently, there is a rapid development to introduce artificial intelligence (AI) methods for improved acquisition, processing and interpretation of MRI [207]. Several AI methods

have already been applied to MRSI of the brain to estimate tissue concentration of metabolites [208, 209], to enhance spatial resolution of MRSI [210] and to assess MRSI spectral quality and filter artifacts [211, 212]. Specifically for prostate MRSI, the application of AI may also be of interest for optimal OVS to suppress lipid signals [213–215].

With SNR being critical in clinical MRSI, the application of denoising methods has attracted much attention recently. A popular approach is low-rank denoising, which is performed by arranging the measured data in matrix forms (i.e., Casorati and Hankel) and applying low-rank approximations by singular value decomposition (SVD). The method can effectively denoise MRSI data over a wide range of SNR values while preserving spatial-spectral features [216, 217]. Also, methodologies incorporating pre-learned spectral basis sets and spatial priors in low-rank approximation methods [218] and principal components analyses (PCA) [219] may be of interest for prostate ^1H MRSI, and also multi-nuclear (^{31}P , ^{13}C) MRSI applications [220].

All these new methods may significantly improve the effective SNR of multidimensional ^1H MRS. As this can be translated to faster measurements and improved spatial resolution, this can help to overcome some final hurdles in prostate MRSI towards clinical application, in particular if data processing steps are automated, ideally in an mpMRI integrated AI algorithm.

A recent multicenter study evaluating PIRADS scoring of mpMRI with an AI-based attention mapping system only showed marginal improvements in PCa detection [221]. One reason may be that the information content of mpMRI data is simply not sufficient for AI methods and that additional imaging information is needed, which may include that of MRSI. For the classification of MR spectra from voxels to PCa detection, lesion location and grades, machine learning approaches have been applied [82, 94, 111, 174, 187, 222–225], essentially using histopathological analysis of whole mount prostatectomy or of image-guided acquired biopsy specimens as gold standard. Training and validation of these AI methods is not trivial as it requires a substantial amount of annotated MRSI data, although convolutional neuronal networks dedicated to limited MRSI data sets have been developed to predict brain tumor grades and other brain diseases [226]. Sharing data may be a solution to this problem [227]. A remaining issue in validation of all these methods is accurate matching of MR(S)I data to histopathological standards of reference (either MR-guided biopsies or whole-mount section histopathology of resected prostates).

Current prostate diagnostics by mpMRI relies on a histopathological tumor classification which has been developed more than 40 years ago [5]. In the diagnosis of brain tumors classical histopathology has been largely replaced by a classification based on molecular markers to discriminate among tumor subtypes [228]. This is now also practiced in

MRI diagnoses of these tumors and has opened new possibilities for MRSI to assist in precision diagnosis, which is most obvious in the identification of IDH1 mutations by 2-hydroxyglutamate [229]. Although no such metabolite has been detected yet for PCa, specific metabolite patterns may be related to genetic molecular or liquid biopsy markers of clinical significance [230] and used to assist in a more personalized diagnosis and treatment.

Most MR biomarkers to identify and characterize PCa rely on a decrease of signal intensity (T2, DWI (ADC), citrate, spermine). This is not ideal as it may not be specific enough. Imaging methods in which signals increase because of cancer presence such as in choline MR imaging and PET imaging would be better suited. Adding ^{68}Ga PSMA PET imaging to mpMRI in a PET/MR system has been proposed to improve the low specificity of mpMRI in the detection of clinically significant prostate cancer [231]. Although expensive PCa diagnosis by PET imaging is in full development [232] it would be of interest to compare its performance to mpMRI including ^1H MRSI. If MRSI could replace PET in this approach, it would prevent a large overload in examination costs and patient burden.

Acknowledgements For the realization of this manuscript, funding was received from the European Union's Horizon 2020 research and innovation program by the Marie-Sklodowska-Curie Grant 813120 (project INSPiRE-MED). We thank Neda Gholizadeh and Saad Ramadan for providing material for Fig. 4.

Author contributions All authors contributed to the conceptualization, literature search, drafting and revising of the manuscript.

Conflict of interest The authors of this manuscript declare no relationships with any companies, whose products or services may be related to the subject matter of the article.

Open Access This article is licensed under a Creative Commons Attribution 4.0 International License, which permits use, sharing, adaptation, distribution and reproduction in any medium or format, as long as you give appropriate credit to the original author(s) and the source, provide a link to the Creative Commons licence, and indicate if changes were made. The images or other third party material in this article are included in the article's Creative Commons licence, unless indicated otherwise in a credit line to the material. If material is not included in the article's Creative Commons licence and your intended use is not permitted by statutory regulation or exceeds the permitted use, you will need to obtain permission directly from the copyright holder. To view a copy of this licence, visit <http://creativecommons.org/licenses/by/4.0/>.

References

1. Sung H, Ferlay J, Siegel RL, Laversanne M, Soerjomataram I, Jemal A, Bray F (2021) Global Cancer Statistics 2020: GLOBOCAN estimates of incidence and mortality worldwide for 36 cancers in 185 countries. *CA Cancer J Clin*. <https://doi.org/10.3322/caac.21660>

2. Culp MBB, Soerjomataram I, Efstathiou JA, Bray F, Jemal A (2020) Recent global patterns in prostate cancer incidence and mortality rates. *Eur Urol*. <https://doi.org/10.1016/j.eururo.2019.08.005>
3. Wong MCS, Goggins WB, Wang HHX, Fung FDH, Leung C, Wong SYS, Ng CF, Sung JY (2016) Global incidence and mortality for prostate cancer: analysis of temporal patterns and trends in 36 countries. *Eur Urol*. <https://doi.org/10.1016/j.eururo.2016.05.043>
4. Tsodikov A, Gulati R, Heijnsdijk EAM, Pinsky PF, Moss SM, Qiu S, De Carvalho TM, Hugosson J, Berg CD, Auvinen A, Andriole GL, Roobol MJ, Crawford ED, Nelen V, Kwiatkowski M, Zappa M, Luján M, Villers A, Feuer EJ, De Koning HJ, Mariotto AB, Etzioni R (2017) Reconciling the effects of screening on prostate cancer mortality in the ERSPC and PLCO trials. *Ann Intern Med*. <https://doi.org/10.7326/M16-2586>
5. Etzioni R, Tsodikov A, Mariotto A, Szabo A, Falcon S, Weigel J, Ditommaso D, Karnofski K, Gulati R, Penson DF, Feuer E (2008) Quantifying the role of PSA screening in the US prostate cancer mortality decline. *Cancer Causes Control*. <https://doi.org/10.1007/s10552-007-9083-8>
6. Center MM, Jemal A, Lortet-Tieulent J, Ward E, Ferlay J, Brawley O, Bray F (2012) International variation in prostate cancer incidence and mortality rates. *Eur Urol*. <https://doi.org/10.1016/j.eururo.2012.02.054>
7. Zlotta AR, Egawa S, Pushkar D, Govorov A, Kimura T, Kido M, Takahashi H, Kuk C, Kovylyna M, Aldaoud N, Fleschner N, Finelli A, Klotz L, Sykes J, Lockwood G, Van Der Kwast TH (2013) Prevalence of prostate cancer on autopsy: cross-sectional study on unscreened Caucasian and Asian men. *J Natl Cancer Inst*. <https://doi.org/10.1093/jnci/djt151>
8. Litwin MS, Tan HJ (2017) The diagnosis and treatment of prostate cancer: a review. *J Am Med Assoc*. <https://doi.org/10.1001/jama.2017.7248>
9. Humphrey PA (2017) Histopathology of prostate cancer. *Cold Spring Harb Perspect Med*. <https://doi.org/10.1101/cshperspect.a030411>
10. Epstein JI, Zelefsky MJ, Sjoberg DD, Nelson JB, Egevad L, Magi-Galluzzi C, Vickers AJ, Parwani AV, Reuter VE, Fine SW, Eastham JA, Wiklund P, Han M, Reddy CA, Ciezki JP, Nyberg T, Klein EA (2016) A contemporary prostate cancer grading system: a validated alternative to the Gleason score. *Eur Urol*. <https://doi.org/10.1016/j.eururo.2015.06.046>
11. Kasivisvanathan V, Rannikko AS, Borghi M, Panebianco V, Mynderse LA, Vaarala MH, Briganti A, Budäus L, Hellawell G, Hindley RG, Roobol MJ, Eggen S, Ghei M, Villers A, Bladou F, Villeirs GM, Virdi J, Boxler S, Robert G, Singh PB, Venderink W, Hadaschik BA, Ruffion A, Hu JC, Margolis D, Crouzet S, Klotz L, Taneja SS, Pinto P, Gill I, Allen C, Giganti F, Freeman A, Morris S, Punwani S, Williams NR, Brew-Graves C, Deeks J, Takwoingi Y, Emberton M, Moore CM (2018) MRI-targeted or standard biopsy for prostate-cancer diagnosis. *N Engl J Med*. <https://doi.org/10.1056/nejmoa1801993>
12. Hoeks CMA, Barentsz JO, Hambroek T, Yakar D, Somford DM, Heijmink SWTPJ, Scheenen TWJ, Vos PC, Huisman H, Van Oort IM, Witjes JA, Heerschap A, Fütterer JJ (2011) Prostate cancer: multiparametric MR imaging for detection, localization, and staging. *Radiology*. <https://doi.org/10.1148/radiol.11091822>
13. Weinreb JC, Barentsz JO, Choyke PL, Cornud F, Haider MA, Macura KJ, Margolis D, Schnall MD, Shtern F, Tempny CM, Thoeny HC, Verma S (2016) PI-RADS prostate imaging—reporting and data system: 2015, version 2. *Eur Urol*. <https://doi.org/10.1016/j.eururo.2015.08.052>
14. Barentsz JO, Richenberg J, Clements R, Choyke P, Verma S, Villeirs G, Rouviere O, Logager V, Fütterer JJ (2012) ESUR prostate MR guidelines 2012. *Eur Radiol*. <https://doi.org/10.1007/s00330-011-2377-y>
15. Stabile A, Giganti F, Kasivisvanathan V, Giannarini G, Moore CM, Padhani AR, Panebianco V, Rosenkrantz AB, Salomon G, Turkbey B, Villeirs G, Barentsz JO (2020) Factors influencing variability in the performance of multiparametric magnetic resonance imaging in detecting clinically significant prostate cancer: a systematic literature review. *Eur Urol Oncol*. <https://doi.org/10.1016/j.euo.2020.02.005>
16. Stabile A, Giganti F, Rosenkrantz AB, Taneja SS, Villeirs G, Gill IS, Allen C, Emberton M, Moore CM, Kasivisvanathan V (2020) Multiparametric MRI for prostate cancer diagnosis: current status and future directions. *Nat Rev Urol*. <https://doi.org/10.1038/s41585-019-0212-4>
17. Tayari N, Heerschap A, Scheenen TWJ, Kobus T (2017) In vivo MR spectroscopic imaging of the prostate, from application to interpretation. *Anal Biochem*. <https://doi.org/10.1016/j.ab.2017.02.001>
18. Payne GS (2018) Clinical applications of in vivo magnetic resonance spectroscopy in oncology. *Phys Med Biol*. <https://doi.org/10.1088/1361-6560/aae61e>
19. Kurhanewicz J, Vigneron DB (2016) Magnetic Resonance Spectroscopy of Prostate Cancer. *eMagRes* 5
20. Kobus T, Wright AJ, Scheenen TWJ, Heerschap A (2014) Mapping of prostate cancer by 1H MRSI. *NMR Biomed*. <https://doi.org/10.1002/nbm.2973>
21. Drost FJH, Osses D, Nieboer D, Bangma CH, Steyerberg EW, Roobol MJ, Schoots IG (2020) Prostate magnetic resonance imaging, with or without magnetic resonance imaging-targeted biopsy, and systematic biopsy for detecting prostate cancer: a cochrane systematic review and meta-analysis. *Eur Urol*. <https://doi.org/10.1016/j.eururo.2019.06.023>
22. Smith CP, Harmon SA, Barrett T, Bittencourt LK, Law YM, Shebel H, An JY, Czarniecki M, Mehralivand S, Coskun M, Wood BJ, Pinto PA, Shih JH, Choyke PL, Turkbey B (2019) Intra- and interreader reproducibility of PI-RADSv2: a multireader study. *J Magn Reson Imaging*. <https://doi.org/10.1002/jmri.26555>
23. American College of Radiology (2015) PI-RADS v2 prostate—prostate imaging and reporting and data system: version 2. *J Chem Inf Model*. <https://doi.org/10.1016/j.eururo.2015.08.052>
24. Kobus T, Wright AJ, Weiland E, Heerschap A, Scheenen TWJ (2015) Metabolite ratios in 1H MR spectroscopic imaging of the prostate. *Magn Reson Med*. <https://doi.org/10.1002/mrm.25122>
25. Sharma U, Jagannathan NR (2020) Metabolism of prostate cancer by magnetic resonance spectroscopy (MRS). *Biophys Rev*. <https://doi.org/10.1007/s12551-020-00758-6>
26. Jagannathan NR (2014) Towards early diagnosis and assessment of cancer: role of MRI and in-vivo MR spectroscopy (MRS). *Ann Natl Acad Med Sci* 50(3&4):135–150
27. Spencer NG, Eykyn TR, DeSouza NM, Payne GS (2010) The effect of experimental conditions on the detection of spermine in cell extracts and tissues. *NMR Biomed*. <https://doi.org/10.1002/nbm.1438>
28. Steinseifer IK, Van Asten JJA, Weiland E, Scheenen TWJ, Maas MC, Heerschap A (2015) Improved volume selective 1H MR spectroscopic imaging of the prostate with gradient offset independent adiabaticity pulses at 3 tesla. *Magn Reson Med*. <https://doi.org/10.1002/mrm.25476>
29. Basharat M, Jafar M, deSouza NM, Payne GS (2014) Evaluation of short-TE 1H MRSI for quantification of metabolites in the prostate. *NMR Biomed*. <https://doi.org/10.1002/nbm.3082>
30. Scheenen TWJ, Gambarota G, Weiland E, Klomp DWJ, Fütterer JJ, Barentsz JO, Heerschap A (2005) Optimal timing for

- in vivo 1H-MR spectroscopic imaging of the human prostate at 3T. *Magn Reson Med.* <https://doi.org/10.1002/mrm.20468>
31. Bales JR, Higham DP, Howe I, Nicholson JK, Sadler PJ (1984) Use of high-resolution proton nuclear magnetic resonance spectroscopy for rapid multi-component analysis of urine. *Clin Chem.* <https://doi.org/10.1093/clinchem/30.3.426>
 32. Van Der Graaf M, Heerschap A (1996) Effect of cation binding on the proton chemical shifts and the spin-spin coupling constant of citrate. *J Magn Reson Ser B.* <https://doi.org/10.1006/jmrb.1996.0109>
 33. Heerschap A, Jager GJ, Van Der Graaf M, Barentsz JO, Ruijs SHJ (1997) Proton MR spectroscopy of the normal human prostate with an endorectal coil and a double spin-echo pulse sequence. *Magn Reson Med.* <https://doi.org/10.1002/mrm.1910370212>
 34. Willker W, Flögel U, Leibfritz D (1998) A 1H/13C inverse 2D method for the analysis of the polyamines putrescine, spermidine and spermine in cell extracts and biofluids. *NMR Biomed.* [https://doi.org/10.1002/\(SICI\)1099-1492\(199804\)11:2%3c47::AID-NBM500%3e3.0.CO;2-G](https://doi.org/10.1002/(SICI)1099-1492(199804)11:2%3c47::AID-NBM500%3e3.0.CO;2-G)
 35. Lagemaat MW, Breukels V, Vos EK, Kerr AB, Van Uden MJ, Orzada S, Bitz AK, Maas MC, Scheenen TWJ (2016) 1H MR spectroscopic imaging of the prostate at 7T using spectral-spatial pulses. *Magn Reson Med.* <https://doi.org/10.1002/mrm.25569>
 36. Lynch MJ, Nicholson JK (1997) Proton MRS of human prostatic fluid: Correlations between citrate, spermine, and myo-inositol levels and changes with disease. *Prostate.* [https://doi.org/10.1002/\(SICI\)1097-0045\(19970301\)30:4%3c248::AID-PROS4%3e3.0.CO;2-H](https://doi.org/10.1002/(SICI)1097-0045(19970301)30:4%3c248::AID-PROS4%3e3.0.CO;2-H)
 37. Costello LC, Franklin RB, Narayan P (1999) Citrate in the diagnosis of prostate cancer. *Prostate.* [https://doi.org/10.1002/\(SICI\)1097-0045\(19990215\)38:3%3c237::AID-PROS8%3e3.0.CO;2-O](https://doi.org/10.1002/(SICI)1097-0045(19990215)38:3%3c237::AID-PROS8%3e3.0.CO;2-O)
 38. Bader DA, McGuire SE (2020) Tumour metabolism and its unique properties in prostate adenocarcinoma. *Nat Rev Urol.* <https://doi.org/10.1038/s41585-020-0288-x>
 39. Costello LC, Franklin RB (1991) Concepts of citrate production and secretion by prostate I. Metabolic relationships. *Prostate.* <https://doi.org/10.1002/pros.2990180104>
 40. Costello LC, Franklin RB (1998) Novel role of zinc in the regulation of prostate citrate metabolism and its implications in prostate cancer. *Prostate.* [https://doi.org/10.1002/\(SICI\)1097-0045\(19980601\)35:4%3c285::AID-PROS8%3e3.0.CO;2-F](https://doi.org/10.1002/(SICI)1097-0045(19980601)35:4%3c285::AID-PROS8%3e3.0.CO;2-F)
 41. Ferramosca A, Zara V (2014) Bioenergetics of mammalian sperm capacitation. *Biomed Res Int.* <https://doi.org/10.1155/2014/902953>
 42. Verze P, Cai T, Lorenzetti S (2016) The role of the prostate in male fertility, health and disease. *Nat Rev Urol.* <https://doi.org/10.1038/nrurol.2016.89>
 43. Mycielska ME, Patel A, Rizaner N, Mazurek MP, Keun H, Patel A, Ganapathy V, Djamgoz MBA (2009) Citrate transport and metabolism in mammalian cells: prostate epithelial cells and prostate cancer. *BioEssays.* <https://doi.org/10.1002/bies.080137>
 44. Kavanagh JP (1985) Sodium, potassium, calcium, magnesium, zinc, citrate and chloride content of human prostatic and seminal fluid. *J Reprod Fertil.* <https://doi.org/10.1530/jrf.0.0750035>
 45. Serkova NJ, Gamito EJ, Jones RH, O'Donnell C, Brown JL, Green S, Sullivan H, Hedlund T, Crawford ED (2008) The metabolites citrate, myo-inositol, and spermine are potential age-independent markers of prostate cancer in human expressed prostatic secretions. *Prostate.* <https://doi.org/10.1002/pros.20727>
 46. Weis J, Ortiz-Nieto F, Ahlström H (2013) MR spectroscopy of the prostate at 3T: measurements of relaxation times and quantification of prostate metabolites using water as an internal reference. *Magn Reson Med Sci.* <https://doi.org/10.2463/mrms.2013-0017>
 47. Lowry M, Liney GP, Turnbull LW, Manton DJ, Blackband SJ, Horsman A (1996) Quantification of citrate concentration in the prostate by proton magnetic resonance spectroscopy: zonal and age-related differences. *Magn Reson Med.* <https://doi.org/10.1002/mrm.1910360305>
 48. Liney GP, Turnbull LW, Lowry M, Turnbull LS, Knowles AJ, Horsman A (1997) In vivo quantification of citrate concentration and water T2 relaxation time of the pathologic prostate gland using 1H MRS and MRI. *Magn Reson Imaging.* [https://doi.org/10.1016/S0730-725X\(97\)00182-3](https://doi.org/10.1016/S0730-725X(97)00182-3)
 49. Swanson MG, Zektzer AS, Tabatabai ZL, Simko J, Jarso S, Keshari KR, Schmitt L, Carroll PR, Shinohara K, Vigneron DB, Kurhanewicz J (2006) Quantitative analysis of prostate metabolites using 1H HR-MAS spectroscopy. *Magn Reson Med.* <https://doi.org/10.1002/mrm.20909>
 50. Swanson MG, Vigneron DB, Tabatabai ZL, Males RG, Schmitt L, Carroll PR, James JK, Hurd RE, Kurhanewicz J (2003) Proton HR-MAS spectroscopy and quantitative pathologic analysis of MRI/3D-MRSI-targeted postsurgical prostate tissues. *Magn Reson Med.* <https://doi.org/10.1002/mrm.10614>
 51. Condorelli RA, La Vignera S, Mongioi LM, Vitale SG, Laganà AS, Cimino L, Calogero AE (2017) Myo-inositol as a male fertility molecule: speed them up! *Eur Rev Med Pharmacol Sci* 21(2 Suppl):30–35
 52. Van Der Graaf M, Schipper RG, Oosterhof GON, Schalken JA, Verhofstad AAJ, Heerschap A (2000) Proton MR spectroscopy of prostatic tissue focused on the detection of spermine, a possible biomarker of malignant behavior in prostate cancer. *Magn Reson Mater Physics, Biol Med.* [https://doi.org/10.1016/S1352-8661\(00\)00082-X](https://doi.org/10.1016/S1352-8661(00)00082-X)
 53. Cohen RJ, Fujiwara K, Holland JW, McNeal JE (2001) Polyamines in prostatic epithelial cells and adenocarcinoma; the effects of androgen blockade. *Prostate.* <https://doi.org/10.1002/pros.10023>
 54. Lefèvre PLC, Palin MF, Murphy BD (2011) Polyamines on the reproductive landscape. *Endocr Rev.* <https://doi.org/10.1210/er.2011-0012>
 55. Cheng LL, Lee WC, Smith MR, Gonzalez RG (2001) Non-destructive quantitation of spermine in human prostate tissue samples using HRMAS 1H NMR spectroscopy at 9.4 T. *FEBS Lett.* [https://doi.org/10.1016/S0014-5793\(01\)02329-8](https://doi.org/10.1016/S0014-5793(01)02329-8)
 56. Jupin M, Van Heijster FHA, Heerschap A (2022) Metabolite interactions in prostatic fluid mimics assessed by 1H NMR. *Magma Magn Reson Mater Physics Biol Med.* <https://doi.org/10.1007/s10334-021-00983-4>
 57. Andersen MK, Høiem TS, Claes BSR, Balluff B, Martin-Lorenzo M, Richardsen E, Krossa S, Bertilsson H, Heeren RMA, Rye MB, Giskeødegård GF, Bathen TF, Tessem M-B (2021) Spatial differentiation of metabolism in prostate cancer tissue by MALDI-TOF MSI. *Cancer Metab.* <https://doi.org/10.1186/s40170-021-00242-z>
 58. Tomlins AM, Foxall PJD, Lynch MJ, Parkinson J, Everett JR, Nicholson JK (1998) High resolution 1H NMR spectroscopic studies on dynamic biochemical processes in incubated human seminal fluid samples. *Biochim Biophys Acta Gen Subj.* [https://doi.org/10.1016/S0304-4165\(97\)00116-5](https://doi.org/10.1016/S0304-4165(97)00116-5)
 59. Reynolds S, Calvert SJ, Paley MN, Pacey AA (2017) 1H magnetic resonance spectroscopy of live human sperm. *Mol Hum Reprod.* <https://doi.org/10.1093/molehr/gax025>
 60. Lagemaat MW, Vos EK, Maas MC, Bitz AK, Orzada S, Van Uden MJ, Kobus T, Heerschap A, Scheenen TWJ (2014) Phosphorus magnetic resonance spectroscopic imaging at 7 T in patients with prostate cancer. *Invest Radiol.* <https://doi.org/10.1097/RLI.0000000000000012>

61. Cooper JF, Farid I (1963) The role of citric acid in the physiology of the prostate. A chromatographic study of citric acid cycle intermediates in benign and malignant prostatic tissue. *J Surg Res.* [https://doi.org/10.1016/S0022-4804\(63\)80041-4](https://doi.org/10.1016/S0022-4804(63)80041-4)
62. Sillerud LO, Halliday KR, Griffey RH, Fenoglio-Preiser C, Shephard S (1988) In vivo ¹³C NMR spectroscopy of the human prostate. *Magn Reson Med.* <https://doi.org/10.1002/mrm.1910080213>
63. Fowler AH, Pappas AA, Holder JC, Finkbeiner AE, Dalrymple GV, Mullins MS, Sprigg JR, Komoroski RA (1992) Differentiation of human prostate cancer from benign hypertrophy by in vitro ¹H NMR. *Magn Reson Med.* <https://doi.org/10.1002/mrm.1910250114>
64. Kurhanewicz J, Dahiya R, Macdonald JM, Chang L-H, James TL, Narayan P (1993) Citrate alterations in primary and metastatic human prostatic adenocarcinomas: ¹H magnetic resonance spectroscopy and biochemical study. *Magn Reson Med.* <https://doi.org/10.1002/mrm.1910290202>
65. Schiebler ML, Miyamoto KK, White M, Maygarden SJ, Mohler JL (1993) In vitro high resolution ¹H-spectroscopy of the human prostate: benign prostatic hyperplasia, normal peripheral zone and adenocarcinoma. *Magn Reson Med.* <https://doi.org/10.1002/mrm.1910290302>
66. Cornel EB, Smits GAHJ, Oosterhof GON, Karthaus HFM, Debruyne FMJ, Schalken JA, Heerschap A (1993) Characterization of human prostate cancer, benign prostatic hyperplasia and normal prostate by in vitro ¹H and ³¹P magnetic resonance spectroscopy. *J Urol.* [https://doi.org/10.1016/S0022-5347\(17\)35957-8](https://doi.org/10.1016/S0022-5347(17)35957-8)
67. Schick F, Bogers H, Kurz S, Jung W-I, Pfeffer M, Lutz O (1993) Localized proton MR spectroscopy of citrate in vitro and of the human prostate in vivo at 1.5 T. *Magn Reson Med.* <https://doi.org/10.1002/mrm.1910290109>
68. Costello LC, Franklin RB (1994) Bioenergetic theory of prostate malignancy. *Prostate.* <https://doi.org/10.1002/pros.2990250308>
69. Langer DL, Van Der Kwast TH, Evans AJ, Plotkin A, Trachtenberg J, Wilson BC, Haider MA (2010) Prostate tissue composition and MR measurements: investigating the relationships between ADC, T2, Ktrans, Ve, and corresponding histologic features. *Radiology.* <https://doi.org/10.1148/radiol.10091343>
70. Kobus T, Van Der Laak JAWM, Maas MC, Hambrock T, Bruggink CC, Hulsbergen-Van De Kaa CA, Scheenen TWJ, Heerschap A (2016) Contribution of histopathologic tissue composition to quantitative MR spectroscopy and diffusion-weighted imaging of the prostate. *Radiology.* <https://doi.org/10.1148/radiol.2015142889>
71. Van Asten JJA, Cuijpers V, Hulsbergen-Van De Kaa C, Soede-Huijbregts C, Witjes JA, Verhofstad A, Heerschap A (2008) High resolution magic angle spinning NMR spectroscopy for metabolic assessment of cancer presence and Gleason score in human prostate needle biopsies. *Magn Reson Mater Physics Biol Med.* <https://doi.org/10.1007/s10334-008-0156-9>
72. Smith RC, Litwin MS, Lu Y, Zetter BR (1995) Identification of an endogenous inhibitor of prostatic carcinoma cell growth. *Nat Med.* <https://doi.org/10.1038/nm1095-1040>
73. Peng Q, Wong CYP, Cheuk IWY, Teoh JYC, Chiu PKF, Ng CF (2021) The emerging clinical role of spermine in prostate cancer. *Int J Mol Sci.* <https://doi.org/10.3390/ijms22094382>
74. Mohan RR, Challa A, Gupta S, Bostwick DG, Ahmad N, Agarwal R, Marengo SR, Amini SB, Paras F, MacLennan GT, Resnick MI, Mukhtar H (1999) Overexpression of ornithine decarboxylase in prostate cancer and prostatic fluid in humans. *Clin Cancer Res* 5(1):143–147
75. Holub BJ (1986) Metabolism and function of myo-inositol and inositol phospholipids. *Annu Rev Nutr.* <https://doi.org/10.1146/annurev.nutr.6.1.563>
76. Bancroft Brown J, Sriram R, VanCriekeing M, Delos Santos R, Sun J, Delos Santos J, Tabatabai ZL, Shinohara K, Nguyen H, Peehl DM, Kurhanewicz J (2019) NMR quantification of lactate production and efflux and glutamate fractional enrichment in living human prostate biopsies cultured with [1,6-¹³C₂]glucose. *Magn Reson Med.* <https://doi.org/10.1002/mrm.27739>
77. Kobus T, Wright AJ, Van Asten JJA, Heerschap A, Scheenen TWJ (2014) In vivo ¹H MR spectroscopic imaging of aggressive prostate cancer: can we detect lactate? *Magn Reson Med.* <https://doi.org/10.1002/mrm.24635>
78. Awwad HM, Geisel J, Obeid R (2012) The role of choline in prostate cancer. *Clin Biochem.* <https://doi.org/10.1016/j.clinbiochem.2012.08.012>
79. Bertilsson H, Tessem MB, Flatberg A, Viset T, Gribbestad I, Angelsen A, Halgunset J (2012) Changes in gene transcription underlying the aberrant citrate and choline metabolism in human prostate cancer samples. *Clin Cancer Res.* <https://doi.org/10.1158/1078-0432.CCR-11-2929>
80. Glunde K, Bhujwala ZM, Ronen SM (2011) Choline metabolism in malignant transformation. *Nat Rev Cancer.* <https://doi.org/10.1038/nrc3162>
81. Tayari N, Steinseifer IK, Selnæs KM, Bathen TF, Maas MC, Heerschap A (2017) High-quality 3-dimensional ¹H magnetic resonance spectroscopic imaging of the prostate without endorectal receive coil using a semi-LASER sequence. *Invest Radiol.* <https://doi.org/10.1097/RLI.0000000000000395>
82. Gholizadeh N, Greer PB, Simpson J, Fu C, Al-iedani O, Lau P, Heerschap A, Ramadan S (2019) Supervised risk predictor of central gland lesions in prostate cancer using ¹H MR spectroscopic imaging with gradient offset-independent adiabaticity pulses. *J Magn Reson Imaging.* <https://doi.org/10.1002/jmri.26803>
83. Starobinets O, Simko JP, Kuchinsky K, Kornak J, Carroll PR, Greene KL, Kurhanewicz J, Noworolski SM (2017) Characterization and stratification of prostate lesions based on comprehensive multiparametric MRI using detailed whole-mount histopathology as a reference standard. *NMR Biomed.* <https://doi.org/10.1002/nbm.3796>
84. Casciani E, Poletini E, Bertini L, Emiliozzi P, Amini M, Pansadoro V, Gualdi GF (2004) Prostate cancer: evaluation with endorectal MR imaging and three-dimensional proton MR spectroscopic imaging. *Radiol Med* 108(5–6):530–541
85. Keshari KR, Tsachres H, Iman R, Delos Santos L, Tabatabai ZL, Shinohara K, Vigneron DB, Kurhanewicz J (2011) Correlation of phospholipid metabolites with prostate cancer pathologic grade, proliferative status and surgical stage—impact of tissue environment. *NMR Biomed.* <https://doi.org/10.1002/nbm.1738>
86. Kobus T, Hambrock T, Hulsbergen-Van De Kaa CA, Wright AJ, Barentsz JO, Heerschap A, Scheenen TWJ (2011) In vivo assessment of prostate cancer aggressiveness using magnetic resonance spectroscopic imaging at 3 T with an endorectal coil. *Eur Urol.* <https://doi.org/10.1016/j.eururo.2011.03.002>
87. Maas MC, Litjens GJS, Wright AJ, Attenberger UI, Haider MA, Helbich TH, Kiefer B, Macura KJ, Margolis DJA, Padhani AR, Selnæs KM, Villeirs GM, Fütterer JJ, Scheenen TWJ (2019) A single-arm, multicenter validation study of prostate cancer localization and aggressiveness with a quantitative multiparametric magnetic resonance imaging approach. *Invest Radiol.* <https://doi.org/10.1097/RLI.0000000000000558>
88. Tayari N, Wright AJ, Heerschap A (2021) Absolute choline tissue concentration mapping for prostate cancer localization and characterization using 3D ¹H MRSI without water-signal suppression. *Magn Reson Med.* <https://doi.org/10.1002/mrm.29012>
89. Pretlow TG, Whitehurst GB, Pretlow TP, Hunt RS, Jacobs JM, McKenzie DR, McDaniel HG, Hall LM, Bradley EL

- (1982) Decrease in creatine kinase in human prostatic carcinoma compared to benign prostatic hyperplasia. *Cancer Res* 42(11):4842–4848
90. Shukla-Dave A, Hricak H, Eberhardt SC, Olgac S, Muruganandham M, Scardino PT, Reuter VE, Koutcher JA, Zakian KL (2004) Chronic prostatitis: MR imaging and 1H MR spectroscopic imaging findings—initial observations. *Radiology*. <https://doi.org/10.1148/radiol.2313031391>
 91. Chen AP, Cunningham CH, Kurhanewicz J, Xu D, Hurd RE, Pauly JM, Carvajal L, Karpodinis K, Vigneron DB (2006) High-resolution 3D MR spectroscopic imaging of the prostate at 3 T with the MLEV-PRESS sequence. *Magn Reson Imaging*. <https://doi.org/10.1016/j.mri.2006.03.002>
 92. Steensma BR, Luttje M, Voogt IJ, Klomp DWJ, Luijten PR, van den Berg CAT, Raaijmakers AJE (2019) Comparing signal-to-noise ratio for prostate imaging at 7T and 3T. *J Magn Reson Imaging*. <https://doi.org/10.1002/jmri.26527>
 93. Tenbergen CJA, Metzger GJ, Scheenen TWJ (2022) Ultra-high field MR in prostate cancer: feasibility and potential. *Magma Magn Reson Mater Physics Biol Med* (submitted)
 94. Lagemaat MW, Philips BWJ, Vos EK, Van Uden MJ, Fütterer JJ, Jenniskens SF, Scheenen TWJ, Maas MC (2017) Feasibility of multiparametric magnetic resonance imaging of the prostate at 7 T. *Invest Radiol*. <https://doi.org/10.1097/RLI.00000000000000342>
 95. Philips BWJ, van Uden MJ, Rietsch SHG, Orzada S, Scheenen TWJ (2019) A multitransmit external body array combined with a 1H and 31P endorectal coil to enable a multiparametric and multimetabolic MRI examination of the prostate at 7T. *Med Phys*. <https://doi.org/10.1002/mp.13696>
 96. Steinseifer IK, Philips BWJ, Gagoski B, Weiland E, Scheenen TWJ, Heerschap A (2017) Flexible proton 3D MR spectroscopic imaging of the prostate with low-power adiabatic pulses for volume selection and spiral readout. *Magn Reson Med*. <https://doi.org/10.1002/mrm.26181>
 97. Thomas MA, Narayan P, Kurhanewicz J, Jajodia P, Weiner MW (1990) 1H MR spectroscopy of normal and malignant human prostates in Vivo. *J Magn Reson*. [https://doi.org/10.1016/0022-2364\(90\)90319-5](https://doi.org/10.1016/0022-2364(90)90319-5)
 98. Kurhanewicz J, Vigneron DB, Hricak H, Narayan P, Carroll P, Nelson SJ (1996) Three-dimensional H-1 MR spectroscopic imaging of the in situ human prostate with high (0.24–0.7 cm³) spatial resolution. *Radiology*. <https://doi.org/10.1148/radiology.198.3.8628874>
 99. Heerschap A, Jager GJ, Van Der Graaf M, Barentsz JO, De La Rosette JJMCH, Oosterhof GON, Ruijter ETG, Ruijs SHJ (1997) In vivo proton MR spectroscopy reveals altered metabolite content in malignant prostate tissue. *Anticancer Res*. 17(3A):1455-60
 100. Kim Y, Hsu ICJ, Pouliot J, Noworolski SM, Vigneron DB, Kurhanewicz J (2005) Expandable and rigid endorectal coils for prostate MRI: impact on prostate distortion and rigid image registration. *Med Phys* doi 10(1118/1):2122467
 101. Noworolski SM, Crane JC, Vigneron DB, Kurhanewicz J (2008) A clinical comparison of rigid and inflatable endorectal-coil probes for MRI and 3D MR spectroscopic imaging (MRSI) of the prostate. *J Magn Reson Imaging*. <https://doi.org/10.1002/jmri.21331>
 102. Vos EK, Sambandamurthy S, Kamel M, Mckenney R, Van Uden MJ, Hoeks CMA, Yakar D, Scheenen TWJ, Fütterer JJ (2014) Clinical comparison between a currently available single-loop and an investigational dual-channel endorectal receive coil for prostate magnetic resonance imaging: a feasibility study at 1.5 and 3 T. *Invest Radiol*. <https://doi.org/10.1097/RLI.0b013e3182a56678>
 103. Choi H, Ma J (2008) Use of perfluorocarbon compound in the endorectal coil to improve MR spectroscopy of the prostate. *Am J Roentgenol*. <https://doi.org/10.2214/AJR.07.2998>
 104. Kaji Y, Wada A, Imaoka I, Matsuo M, Terachi T, Kobashi Y, Sugimura K, Fujii M, Maruyama K, Takizawa O (2002) Proton two-dimensional chemical shift imaging for evaluation of prostate cancer: external surface coil vs endorectal surface coil. *J Magn Reson Imaging*. <https://doi.org/10.1002/jmri.10204>
 105. Lichy MP, Pintaske J, Kottke R, Machann J, Anastasiadis A, Roell S, Hennenlotter J, Diergarten T, Schick F, Stenzl A, Clausen CD, Schlemmer HP (2005) 3D proton MR spectroscopic imaging of prostate cancer using a standard spine coil at 15 T in clinical routine: a feasibility study. *Eur Radiol*. <https://doi.org/10.1007/s00330-004-2547-2>
 106. Scheenen TWJ, Heijmink SWTPJ, Roell SA, Hulsbergen-Van De Kaa CA, Knipscheer BC, Witjes JA, Barentsz JO, Heerschap A (2007) Three-dimensional proton MR spectroscopy of human prostate at 3 T without endorectal coil: feasibility. *Radiology*. <https://doi.org/10.1148/radiol.2451061444>
 107. Yakar D, Heijmink SWTPJ, Hulsbergen-Van De Kaa CA, Huisman H, Barentsz JO, Fütterer JJ, Scheenen TWJ (2011) Initial results of 3-dimensional 1H-magnetic resonance spectroscopic imaging in the localization of prostate cancer at 3 tesla: should we use an endorectal coil? *Invest Radiol*. <https://doi.org/10.1097/RLI.0b013e3182007503>
 108. Shah ZK, Elias SN, Abaza R, Zynger DL, DeRenne LA, Knopp MV, Guo B, Schurr R, Heymsfield SB, Jia G (2015) Performance comparison of 15-T endorectal coil MRI with 30-T nonendorectal coil MRI in patients with prostate cancer. *Acad Radiol*. <https://doi.org/10.1016/j.acra.2014.11.007>
 109. Nagarajan R, Margolis DJ, Raman SS, Ouellette D, Sarma MK, Reiter RE, Thomas MA (2013) MR spectroscopic imaging of peripheral zone in prostate cancer using a 3t MRI scanner: endorectal versus external phased array coils. *Magn Reson Insights*. <https://doi.org/10.4137/mri.s10861>
 110. De Visschere P, Nezzo M, Pattyn E, Fonteyne V, Van Praet C, Villeirs G (2015) Prostate magnetic resonance spectroscopic imaging at 1.5 tesla with endorectal coil versus 3.0 tesla without endorectal coil: comparison of spectral quality. *Clin Imaging*. <https://doi.org/10.1016/j.clinimag.2015.02.008>
 111. Gholizadeh N, Greer PB, Simpson J, Goodwin J, Fu C, Lau P, Siddique S, Heerschap A, Ramadan S (2021) Diagnosis of transition zone prostate cancer by multiparametric MRI: added value of MR spectroscopic imaging with sLASER volume selection. *J Biomed Sci*. <https://doi.org/10.1186/s12929-021-00750-6>
 112. Le Fur Y, Cozzone PJ (2014) FID modulus: a simple and efficient technique to phase and align MR spectra. *Magn Reson Mater Physics Biol Med*. <https://doi.org/10.1007/s10334-013-0381-8>
 113. Le Fur Y, Cozzone PJ (2015) Hemi-spectrum substitution after water signal fitting (HESWAF): an improvement of the modulus post-processing of MR spectra. *Magn Reson Mater Physics Biol Med*. <https://doi.org/10.1007/s10334-014-0444-5>
 114. Stamatelatou A, Sima DM, Van Huffel S, Van Asten JJ, Heerschap A, Scheenen TWJ (2021) Post-acquisition water signal removal in 3D water-unsuppressed 1H-MR spectroscopic imaging data of the prostate. In: Proceedings of the 29th scientific meeting, International Society for Magnetic Resonance in medicine, Vancouver, p 4001
 115. Tenbergen C, Ruhm L, Heerschap A, Henning A, Scheenen T (2020) Over-discretized reconstruction to correct for B0 inhomogeneity and improve localization in 1H-MRSI of the prostate. In: Proceedings of the 28th scientific meeting, International Society for Magnetic Resonance in medicine, Sydney, p 2914
 116. Arnoldner MA, Polanec SH, Lazar M, Khadjavi S, Clauser P, Pötsch N, Schwarz-Nemec U, Korne S, Hübner N, Shariat SF,

- Helbich TH, Baltzer PAT (2022) Rectal preparation significantly improves prostate imaging quality: assessment of the PI-QUAL score with visual grading characteristics. *Eur J Radiol*. <https://doi.org/10.1016/j.ejrad.2021.110145>
117. Frahm J, Merboldt KD, Hänicke W (1987) Localized proton spectroscopy using stimulated echoes. *J Magn Reson*. [https://doi.org/10.1016/0022-2364\(87\)90154-5](https://doi.org/10.1016/0022-2364(87)90154-5)
 118. Bottomley PA (1987) Spatial localization in NMR spectroscopy in vivo. *Ann NY Acad Sci*. <https://doi.org/10.1111/j.1749-6632.1987.tb32915.x>
 119. Zierhut ML, Ozturk-Isik E, Chen AP, Park I, Vigneron DB, Nelson SJ (2009) 1H spectroscopic imaging of human brain at 3 Tesla: comparison of fast three-dimensional magnetic resonance spectroscopic imaging techniques. *J Magn Reson Imaging*. <https://doi.org/10.1002/jmri.21834>
 120. Slotboom J, Bovée WMMJ (1995) Adiabatic slice-selective RF pulses and a single-shot adiabatic localization pulse sequence. *Concepts Magn Reson*. <https://doi.org/10.1002/cmr.1820070303>
 121. Garwood M, DelaBarre L (2001) The return of the frequency sweep: designing adiabatic pulses for contemporary NMR. *J Magn Reson*. <https://doi.org/10.1006/jmre.2001.2340>
 122. Kupce E, Freeman R (1995) Adiabatic pulses for wide-band inversion and broad-band decoupling. *J Magn Reson*. <https://doi.org/10.1006/jmra.1995.1179>
 123. Sacolick LI, Rothman DL, De Graaf RA (2007) Adiabatic refocusing pulses for volume selection in magnetic resonance spectroscopic imaging. *Magn Reson Med*. <https://doi.org/10.1002/mrm.21162>
 124. Andronesi OC, Ramadan S, Ratai EM, Jennings D, Mountford CE, Sorensen AG (2010) Spectroscopic imaging with improved gradient modulated constant adiabaticity pulses on high-field clinical scanners. *J Magn Reson*. <https://doi.org/10.1016/j.jmr.2010.01.010>
 125. Chen AP, Cunningham CH, Ozturk-Isik E, Xu D, Hurd RE, Kelley DAC, Pauly JM, Kurhanewicz J, Nelson SJ, Vigneron DB (2007) High-speed 3T MR spectroscopic imaging of prostate with flyback echo-planar encoding. *J Magn Reson Imaging*. <https://doi.org/10.1002/jmri.20916>
 126. Schricker AA, Pauly JM, Kurhanewicz J, Swanson MG, Vigneron DB (2001) Dualband spectral-spatial RF pulses for prostate MR spectroscopic imaging. *Magn Reson Med*. <https://doi.org/10.1002/mrm.1302>
 127. Klomp DWJ, Scheenen TWJ, Arteaga CS, van Asten J, Boer VO, Luijten PR (2011) Detection of fully refocused polyamine spins in prostate cancer at 7 T. *NMR Biomed*. <https://doi.org/10.1002/nbm.1592>
 128. Gambarota G, Van Der Graaf M, Klomp D, Mulkern RV, Heerschap A (2005) Echo-time independent signal modulations using PRESS sequences: a new approach to spectral editing of strongly coupled AB spin systems. *J Magn Reson*. <https://doi.org/10.1016/j.jmr.2005.08.006>
 129. Yue K, Marumoto A, Binesh N, Thomas MA (2002) 2D JPRESS of human prostates using an endorectal receiver coil. *Magn Reson Med*. <https://doi.org/10.1002/mrm.10160>
 130. Kim DH, Margolis D, Xing L, Daniel B, Spielman D (2005) In vivo prostate magnetic resonance spectroscopic imaging using two-dimensional J-resolved PRESS at 3 T. *Magn Reson Med*. <https://doi.org/10.1002/mrm.20452>
 131. Lange T, Schulte RF, Boesiger P (2008) Quantitative J-resolved prostate spectroscopy using two-dimensional prior-knowledge fitting. *Magn Reson Med*. <https://doi.org/10.1002/mrm.21438>
 132. Nagarajan R, Gomez AM, Raman SS, Margolis DJ, McClure T, Thomas MA (2010) Correlation of endorectal 2D JPRESS findings with pathological Gleason scores in prostate cancer patients. *NMR Biomed*. <https://doi.org/10.1002/nbm.1446>
 133. Nagarajan R, Iqbal Z, Burns B, Wilson NE, Sarma MK, Margolis DA, Reiter RE, Raman SS, Thomas MA (2015) Accelerated echo planar J-resolved spectroscopic imaging in prostate cancer: a pilot validation of non-linear reconstruction using total variation and maximum entropy. *NMR Biomed*. <https://doi.org/10.1002/nbm.3373>
 134. Thomas MA, Nagarajan R, Huda A, Margolis D, Sarma MK, Sheng K, Reiter RE, Raman SS (2014) Multidimensional MR spectroscopic imaging of prostate cancer in vivo. *NMR Biomed*. <https://doi.org/10.1002/nbm.2991>
 135. Furuyama JK, Wilson NE, Burns BL, Nagarajan R, Margolis DJ, Thomas MA (2012) Application of compressed sensing to multidimensional spectroscopic imaging in human prostate. *Magn Reson Med*. <https://doi.org/10.1002/mrm.24265>
 136. Van Der Graaf M, Van Den Boogert HJ, Jager GJ, Barentsz JO, Heerschap A (1999) Human prostate: multisection proton MR spectroscopic imaging with a single spin-echo sequence—preliminary experience. *Radiology*. <https://doi.org/10.1148/radiology.213.3.r99nv07919>
 137. Van der Graaf M, Jager GJ, Heerschap A (1997) Removal of the outer lines of the citrate multiplet in proton magnetic resonance spectra of the prostatic gland by accurate timing of a point-resolved spectroscopy pulse sequence. *Magn Reson Mater Physics Biol Med*. <https://doi.org/10.1007/BF02592268>
 138. Scheenen TWJ, Fütterer J, Weiland E, Van Hecke P, Lemort M, Zechmann C, Schlemmer HP, Broome D, Villeirs G, Lu J, Barentsz J, Roell S, Heerschap A (2011) Discriminating cancer from noncancer tissue in the prostate by 3-dimensional proton magnetic resonance spectroscopic imaging: a prospective multicenter validation study. *Invest Radiol*. <https://doi.org/10.1097/RLI.0b013e3181f54081>
 139. Trabesinger AH, Meier D, Dydak U, Lamerichs R, Boesiger P (2005) Optimizing PRESS localized citrate detection at 3 Tesla. *Magn Reson Med*. <https://doi.org/10.1002/mrm.20544>
 140. Verma S, Rajesh A, Fütterer JJ, Turkbey B, Scheenen TWJ, Pang Y, Choyke PL, Kurhanewicz J (2010) Prostate MRI and 3D MR spectroscopy: how we do it. *Am J Roentgenol*. <https://doi.org/10.2214/AJR.10.4312>
 141. Klomp DWJ, Bitz AK, Heerschap A, Scheenen TWJ (2009) Proton spectroscopic imaging of the human prostate at 7 T. *NMR Biomed*. <https://doi.org/10.1002/nbm.1360>
 142. Near J, Romagnoli C, Bartha R (2009) Reduced power magnetic resonance spectroscopic imaging of the prostate at 4.0 Tesla. *Magn Reson Med*. <https://doi.org/10.1002/mrm.21845>
 143. Schmidt C, Hötker AM, Muehlethaler UJ, Burger IA, Donati OF, Barth BK (2021) Value of bowel preparation techniques for prostate MRI: a preliminary study. *Abdom Radiol*. <https://doi.org/10.1007/s00261-021-03046-3>
 144. Thiel T, Czisch M, Elbel GK, Hennig J (2002) Phase coherent averaging in magnetic resonance spectroscopy using interleaved navigator scans: compensation of motion artifacts and magnetic field instabilities. *Magn Reson Med*. <https://doi.org/10.1002/mrm.10174>
 145. Kim DH, Adalsteinsson E, Spielman DM (2004) Spiral readout gradients for the reduction of motion artifacts in chemical shift imaging. *Magn Reson Med*. <https://doi.org/10.1002/mrm.20004>
 146. Tran TKC, Vigneron DB, Sailasuta N, Tropp J, Le Roux P, Kurhanewicz J, Nelson S, Hurd R (2000) Very selective suppression pulses for clinical MRSI studies of brain and prostate cancer. *Magn Reson Med*. [https://doi.org/10.1002/\(SICI\)1522-2594\(200001\)43:1%3c23::AID-MRM4%3e3.0.CO;2-E](https://doi.org/10.1002/(SICI)1522-2594(200001)43:1%3c23::AID-MRM4%3e3.0.CO;2-E)
 147. Venugopal N, McCurdy B, Al Mehairi S, Alamri A, Sandhu GS, Sivalingam S, Drachenberg D, Ryner L (2012) Short echo time in vivo prostate 1H-MRSI. *Magn Reson Imaging*. <https://doi.org/10.1016/j.mri.2011.09.020>

148. Venugopal N, Mccurdy B, Hovdebo J, Al Mehairi S, Alamri A, Sandhu GS, Sivalingam S, Drachenberg D, Ryner L (2012) Automatic conformal prescription of very selective saturation bands for in vivo 1H-MRSI of the prostate. *NMR Biomed.* <https://doi.org/10.1002/nbm.1780>
149. Wang B, Lei Y, Tian S, Wang T, Liu Y, Patel P, Jani AB, Mao H, Curran WJ, Liu T, Yang X (2019) Deeply supervised 3D fully convolutional networks with group dilated convolution for automatic MRI prostate segmentation. *Med Phys.* <https://doi.org/10.1002/mp.13416>
150. Males RG, Vigneron DB, Star-Lack J, Falbo SC, Nelson SJ, Hricak H, Kurhanewicz J (2000) Clinical application of BASING and spectral/spatial water and lipid suppression pulses for prostate cancer staging and localization by in vivo 3D 1H magnetic resonance spectroscopic imaging. *Magn Reson Med.* [https://doi.org/10.1002/\(SICI\)1522-2594\(200001\)43:1%3c17::AID-MRM3%3e3.0.CO;2-6](https://doi.org/10.1002/(SICI)1522-2594(200001)43:1%3c17::AID-MRM3%3e3.0.CO;2-6)
151. Star-Lack J, Nelson SJ, Kurhanewicz J, Huang LR, Vigneron DB (1997) Improved water and lipid suppression for 3D PRESS CSI using RF band selective inversion with gradient dephasing (BASING). *Magn Reson Med.* <https://doi.org/10.1002/mrm.1910380222>
152. Mescher M, Tannus A, O'Neil Johnson M, Garwood M (1996) Solvent suppression using selective echo dephasing. *J Magn Reson Ser A.* <https://doi.org/10.1006/jmra.1996.0242>
153. Pohmann R, Von Kienlin M (2001) Accurate phosphorus metabolite images of the human heart by 3D acquisition-weighted CSI. *Magn Reson Med.* <https://doi.org/10.1002/mrm.1110>
154. Scheenen TWJ, Klomp DWJ, Röhl SA, Fütterer JJ, Barentsz JO, Heerschap A (2004) Fast acquisition-weighted three-dimensional proton MR spectroscopic imaging of the human prostate. *Magn Reson Med.* <https://doi.org/10.1002/mrm.20103>
155. Mareci TH, Brooker HR (1991) Essential considerations for spectral localization using indirect gradient encoding of spatial information. *J Magn Reson.* [https://doi.org/10.1016/0022-2364\(91\)90267-W](https://doi.org/10.1016/0022-2364(91)90267-W)
156. Near J, Romagnoli C, Curtis AT, Klassen LM, Izawa J, Chin J, Bartha R (2009) High-field MRSI of the prostate using a transmit/receive endorectal coil and gradient modulated adiabatic localization. *J Magn Reson Imaging.* <https://doi.org/10.1002/jmri.21841>
157. Zakian KL, Sircar K, Hricak H, Chen HN, Shukla-Dave A, Eberhardt S, Muruganandham M, Eboral L, Kattan MW, Reuter VE, Scardino PT, Koutcher JA (2005) Correlation of proton MR spectroscopic imaging with gleason score based on step-section pathologic analysis after radical prostatectomy. *Radiology.* <https://doi.org/10.1148/radiol.2343040363>
158. Jung JA, Coakley FV, Vigneron DB, Swanson MG, Qayyum A, Weinberg V, Jones KD, Carroll PR, Kurhanewicz J (2004) Prostate depiction at endorectal MR spectroscopic imaging: investigation of a standardized evaluation system. *Radiology.* <https://doi.org/10.1148/radiol.2333030672>
159. Weinreb JC, Blume JD, Coakley FV, Wheeler TM, Cormack JB, Sotto CK, Cho H, Kawashima A, Tempny-Afdhal CM, Macura KJ, Rosen M, Gerst SR, Kurhanewicz J (2009) Prostate cancer: sextant localization at MR imaging and MR spectroscopic imaging before prostatectomy—results of ACRIN prospective multi-institutional clinicopathologic study. *Radiology.* <https://doi.org/10.1148/radiol.2511080409>
160. Vareth M, Lupo J, Larson P, Nelson S (2018) A comparison of coil combination strategies in 3D multi-channel MRSI reconstruction for patients with brain tumors. *NMR Biomed.* <https://doi.org/10.1002/nbm.3929>
161. Noworolski SM, Reed GD, Kurhanewicz J, Vigneron DB (2010) Post-processing correction of the endorectal coil reception effects in MR spectroscopic imaging of the prostate. *J Magn Reson Imaging.* <https://doi.org/10.1002/jmri.22258>
162. Nelson SJ, Brown TR (1989) The accuracy of quantification from 1D NMR spectra using the PIQABLE algorithm. *J Magn Reson.* [https://doi.org/10.1016/0022-2364\(89\)90008-5](https://doi.org/10.1016/0022-2364(89)90008-5)
163. Wright AJ, Buydens LMC, Heerschap A (2012) A phase and frequency alignment protocol for 1H MRSI data of the prostate. *NMR Biomed.* <https://doi.org/10.1002/nbm.1790>
164. Wright AJ, Heerschap A (2012) Simple baseline correction for 1H MRSI data of the prostate. *Magn Reson Med.* <https://doi.org/10.1002/mrm.24182>
165. Serrai H, Clayton DB, Senhadji L, Zuo C, Lenkinski RE (2002) Localized proton spectroscopy without water suppression: removal of gradient induced frequency modulations by modulus signal selection. *J Magn Reson.* <https://doi.org/10.1006/jmre.2001.2462>
166. Brown TR, Stoyanova R (1996) NMR spectral quantitation by principal-component analysis. II. Determination of frequency and phase shifts. *J Magn Reson Ser B.* <https://doi.org/10.1006/jmrb.1996.0106>
167. Witjes H, Melssen WJ, Int Zandt HJA, Van Der Graaf M, Heerschap A, Buydens LMC (2000) Automatic correction for phase shifts, frequency shifts, and lineshape distortions across a series of single resonance lines in large spectral data sets. *J Magn Reson.* <https://doi.org/10.1006/jmre.2000.2021>
168. McLean MA, Barrett T, Gnanapragasam VJ, Priest AN, Joubert I, Lomas DJ, Neal DE, Griffiths JR, Sala E (2011) Prostate cancer metabolite quantification relative to water in 1H-MRSI in vivo at 3 Tesla. *Magn Reson Med.* <https://doi.org/10.1002/mrm.22703>
169. García-Martín ML, Adrados M, Ortega MP, Fernández González I, López-Larrubia P, Víaño J, García-Segura JM (2011) Quantitative 1H MR spectroscopic imaging of the prostate gland using LCModel and a dedicated basis-set: correlation with histologic findings. *Magn Reson Med.* <https://doi.org/10.1002/mrm.22631>
170. Provencher SW (1993) Estimation of metabolite concentrations from localized in vivo proton NMR spectra. *Magn Reson Med.* <https://doi.org/10.1002/mrm.1910300604>
171. Shukla-Dave A, Hricak H, Moskowitz C, Ishill N, Akin O, Kuroiwa K, Spector J, Kumar M, Reuter VE, Koutcher JA, Zakian KL (2007) Detection of prostate cancer with MR spectroscopic imaging: an expanded paradigm incorporating polyamines. *Radiology.* <https://doi.org/10.1148/radiol.2452062201>
172. Nelson SJ, Brown TR (1987) A method for automatic quantification of one-dimensional spectra with low signal-to-noise ratio. *J Magn Reson.* [https://doi.org/10.1016/0022-2364\(87\)90033-3](https://doi.org/10.1016/0022-2364(87)90033-3)
173. Pels P, Osturk-Isik E, Swanson MG, Vanhamme L, Kurhanewicz J, Nelson SJ, Van Huffel S (2006) Quantification of prostate MRSI data by model-based time domain fitting and frequency domain analysis. *NMR Biomed.* <https://doi.org/10.1002/nbm.1008>
174. Zechmann CM, Menze BH, Kelm BM, Zamecnik P, Ikingier U, Giesel FL, Thieke C, Delorme S, Hamprecht FA, Bachert P (2012) Automated vs. manual pattern recognition of 3D 1H MRSI data of patients with prostate cancer. *Acad Radiol.* <https://doi.org/10.1016/j.acra.2012.02.014>
175. Prando A, Kurhanewicz J, Borges AP, Oliveira EM, Figueiredo E (2005) Prostatic biopsy directed with endorectal MR spectroscopic imaging findings in patients with elevated prostate specific antigen levels and prior negative biopsy findings: early experience. *Radiology.* <https://doi.org/10.1148/radiol.2363040615>
176. Fütterer JJ, Scheenen TWJ, Heijmink SWTPJ, Huisman HJ, Hulsbergen-Van De Kaa CA, Witjes JA, Heerschap A, Barentsz JO (2007) Standardized threshold approach using three-dimensional proton magnetic resonance spectroscopic imaging in prostate

- cancer localization of the entire prostate. *Invest Radiol.* <https://doi.org/10.1097/01.ri.0000251541.03822.bb>
177. Wetter A, Hübner F, Lehnert T, Fliessbach K, Vorbuchner M, Roell S, Zangos S, Luboldt W, Vogl TJ (2005) Three-dimensional 1H-magnetic resonance spectroscopy of the prostate in clinical practice: technique and results in patients with elevated prostate-specific antigen and negative or no previous prostate biopsies. *Eur Radiol.* <https://doi.org/10.1007/s00330-004-2562-3>
 178. Prando A (2008) Prostate cancer: identification with combined diffusion-weighted MR imaging and 3D 1H MR spectroscopic imaging—correlation with pathologic findings. *Int Braz J Urol.* <https://doi.org/10.1148/radiol.2462070368>
 179. Wright AJ, Kobus T, Selnaes KM, Gribbestad IS, Weiland E, Scheenen TWJ, Heerschap A (2013) Quality control of prostate 1H MRSI data. *NMR Biomed.* <https://doi.org/10.1002/nbm.2835>
 180. Tayari N, Obels J, Kobus T, Scheenen TWJ, Heerschap A (2019) Simple and broadly applicable automatic quality control for 3D 1H MR spectroscopic imaging data of the prostate. *Magn Reson Med.* <https://doi.org/10.1002/mrm.27616>
 181. Provencher SW (2001) Automatic quantitation of localized in vivo 1H spectra with LCMoDel. *NMR Biomed.* <https://doi.org/10.1002/nbm.698>
 182. Vanhamme L, Van Den Boogaart A, Van Huffel S (1997) Improved method for accurate and efficient quantification of MRS data with use of prior knowledge. *J Magn Reson.* <https://doi.org/10.1006/jmre.1997.1244>
 183. Naressi A, Couturier C, Devos JM, Janssen M, Mangeat C, de Beer R, Graveron-Demilly D (2001) Java-based graphical user interface for the MRUI quantitation package. *Magma Magn Reson Mater Physics Biol Med.* <https://doi.org/10.1007/bf02668096>
 184. Wilson M, Reynolds G, Kauppinen RA, Arvanitis TN, Peet AC (2011) A constrained least-squares approach to the automated quantitation of in vivo 1H magnetic resonance spectroscopy data. *Magn Reson Med.* <https://doi.org/10.1002/mrm.22579>
 185. Tayari N, Wright A, Heerschap A (2021) Absolute choline tissue concentration mapping for prostate cancer localization and characterization using 3D 1 H MRSI without water-signal suppression. *Magn Reson Med.* <https://doi.org/10.1002/mrm.29012>
 186. Hamilton EI (1976) Report of the task group on reference man, international commission on radiological protection publication 23. *Sci Total Environ.* [https://doi.org/10.1016/0048-9697\(76\)90016-4](https://doi.org/10.1016/0048-9697(76)90016-4)
 187. Kelm BM, Menze BH, Zechmann CM, Baudendistel KT, Hamprecht FA (2007) Automated estimation of tumor probability in prostate magnetic resonance spectroscopic imaging: pattern recognition vs quantification. *Magn Reson Med.* <https://doi.org/10.1002/mrm.21112>
 188. Giusti S, Caramella D, Fruzzetti E, Lazzereschi M, Tognetti A, Bartolozzi C (2010) Peripheral zone prostate cancer. Pre-treatment evaluation with MR and 3D 1H MR spectroscopic imaging: correlation with pathologic findings. *Abdom Imaging.* <https://doi.org/10.1007/s00261-009-9577-9>
 189. Fusco R, Sansone M, Granata V, Setola SV, Petrillo A (2017) A systematic review on multiparametric MR imaging in prostate cancer detection. *Infect Agent Cancer.* <https://doi.org/10.1186/s13027-017-0168-z>
 190. Villeirs GM, De Meerleer GO, De Visschere PJ, Fonteyne VH, Verbaeys AC, Oosterlinck W (2011) Combined magnetic resonance imaging and spectroscopy in the assessment of high grade prostate carcinoma in patients with elevated PSA: a single-institution experience of 356 patients. *Eur J Radiol.* <https://doi.org/10.1016/j.ejrad.2009.08.007>
 191. Polanec SH, Pinker-Domenig K, Brader P, Georg D, Shariat S, Spick C, Susani M, Helbich TH, Baltzer PA (2016) Multiparametric MRI of the prostate at 3 T: limited value of 3D 1H-MR spectroscopy as a fourth parameter. *World J Urol.* <https://doi.org/10.1007/s00345-015-1670-9>
 192. Wolters T, Roobol MJ, Van Leeuwen PJ, Van Den Bergh RCN, Hoedemaeker RF, Van Leenders GJLH, Schrder FH, Van Der Kwast TH (2011) A critical analysis of the tumor volume threshold for clinically insignificant prostate cancer using a data set of a randomized screening trial. *J Urol.* <https://doi.org/10.1016/j.juro.2010.08.082>
 193. Kobus T, Vos PC, Hambrock T, De Rooij M, Hulsbergen-Van De Kaa CA, Barentsz JO, Heerschap A, Scheenen TWJ (2012) Prostate cancer aggressiveness: in vivo assessment of MR spectroscopy and diffusion-weighted imaging at 3 T. *Radiology.* <https://doi.org/10.1148/radiol.12111744>
 194. Vos EK, Kobus T, Litjens GJS, Hambrock T, Hulsbergen-Van De Kaa CA, Barentsz JO, Maas MC, Scheenen TWJ (2015) Multiparametric magnetic resonance imaging for discriminating low-grade from high-grade prostate cancer. *Invest Radiol.* <https://doi.org/10.1097/RLI.0000000000000157>
 195. Shukla-Dave A, Hricak H, Kattan MW, Pucar D, Kuroiwa K, Chen HN, Spector J, Koutcher JA, Zakian KL, Scardino PT (2007) The utility of magnetic resonance imaging and spectroscopy for predicting insignificant prostate cancer: an initial analysis. *BJU Int.* <https://doi.org/10.1111/j.1464-410X.2007.06689.x>
 196. Mussi TC, Martins T, Garcia RG, Filippi RZ, Lemos GC, Baroni RH (2017) Are dynamic contrast-enhanced images necessary for prostate cancer detection on multiparametric magnetic resonance imaging? *Clin Genitourin Cancer.* <https://doi.org/10.1016/j.clgc.2016.10.001>
 197. De Visschere P, Lumen N, Ost P, Decaestecker K, Pattyn E, Villeirs G (2017) Dynamic contrast-enhanced imaging has limited added value over T2-weighted imaging and diffusion-weighted imaging when using PI-RADSv2 for diagnosis of clinically significant prostate cancer in patients with elevated PSA. *Clin Radiol.* <https://doi.org/10.1016/j.crad.2016.09.011>
 198. Lam F, Liang ZP (2014) A subspace approach to high-resolution spectroscopic imaging. *Magn Reson Med.* <https://doi.org/10.1002/mrm.25168>
 199. Lam F, Ma C, Clifford B, Johnson CL, Liang ZP (2016) High-resolution 1H-MRSI of the brain using SPICE: data acquisition and image reconstruction. *Magn Reson Med.* <https://doi.org/10.1002/mrm.26019>
 200. Klausner A, Strasser B, Thapa B, Lazeyras F, Andronesi O (2021) Achieving high-resolution 1H-MRSI of the human brain with compressed-sensing and low-rank reconstruction at 7 Tesla. *J Magn Reson.* <https://doi.org/10.1016/j.jmr.2021.107048>
 201. Gholizadeh N, Pundavela J, Nagarajan R, Dona A, Quadrelli S, Biswas T, Greer PB, Ramadan S (2020) Nuclear magnetic resonance spectroscopy of human body fluids and in vivo magnetic resonance spectroscopy: potential role in the diagnosis and management of prostate cancer. *Urol Oncol Semin Orig Investig.* <https://doi.org/10.1016/j.urolonc.2019.10.019>
 202. Juchem C, Cudalbu C, de Graaf RA, Gruetter R, Henning A, Hetherington HP, Boer VO (2021) B₀ shimming for in vivo magnetic resonance spectroscopy: experts' consensus recommendations. *NMR Biomed.* <https://doi.org/10.1002/nbm.4350>
 203. Juchem C, de Graaf RA (2017) B₀ magnetic field homogeneity and shimming for in vivo magnetic resonance spectroscopy. *Anal Biochem.* <https://doi.org/10.1016/j.ab.2016.06.003>
 204. De Graaf RA, Juchem C (2016) B₀ shimming technology. *New Dev NMR.* <https://doi.org/10.1039/9781782623878-00166>
 205. Stockmann JP, Wald LL (2018) In vivo B₀ field shimming methods for MRI at 7 T. *Neuroimage.* <https://doi.org/10.1016/j.neuroimage.2017.06.013>
 206. Schwertner M, Hetherington H, Moon CH, Pan J, Felder J, Tellmann L, Shah NJ (2019) Interslice current change constrained B₀ shim optimization for accurate high-order dynamic shim

- updating with strongly reduced eddy currents. *Magn Reson Med*. <https://doi.org/10.1002/mrm.27720>
207. Bardis MD, Houshyar R, Chang PD, Ushinsky A, Glavis-Bloom J, Chahine C, Bui TL, Rupasinghe M, Filippi CG, Chow DS (2020) Applications of artificial intelligence to prostate multiparametric mri (Mpmri): current and emerging trends. *Cancers (Basel)*. <https://doi.org/10.3390/cancers12051204>
 208. Lee HH, Kim H (2019) Intact metabolite spectrum mining by deep learning in proton magnetic resonance spectroscopy of the brain. *Magn Reson Med*. <https://doi.org/10.1002/mrm.27727>
 209. Gurbani SS, Sheriff S, Maudsley AA, Shim H, Cooper LAD (2019) Incorporation of a spectral model in a convolutional neural network for accelerated spectral fitting. *Magn Reson Med*. <https://doi.org/10.1002/mrm.27641>
 210. Iqbal Z, Nguyen D, Hangel G, Motyka S, Bogner W, Jiang S (2019) Super-resolution 1H magnetic resonance spectroscopic imaging utilizing deep learning. *Front Oncol*. <https://doi.org/10.3389/fonc.2019.01010>
 211. Gurbani SS, Schreibmann E, Maudsley AA, Cordova JS, Soher BJ, Poptani H, Verma G, Barker PB, Shim H, Cooper LAD (2018) A convolutional neural network to filter artifacts in spectroscopic MRI. *Magn Reson Med*. <https://doi.org/10.1002/mrm.27166>
 212. Kyathanahally SP, Döring A, Kreis R (2018) Deep learning approaches for detection and removal of ghosting artifacts in MR spectroscopy. *Magn Reson Med*. <https://doi.org/10.1002/mrm.27096>
 213. Iqbal Z, Wilson NE, Thomas MA (2016) 3D spatially encoded and accelerated TE-averaged echo planar spectroscopic imaging in healthy human brain. *NMR Biomed*. <https://doi.org/10.1002/nbm.3469>
 214. Ozhinsky E, Vigneron DB, Nelson SJ (2011) Improved spatial coverage for brain 3D PRESS MRSI by automatic placement of outer-volume suppression saturation bands. *J Magn Reson Imaging*. <https://doi.org/10.1002/jmri.22507>
 215. Nguyen XV, Oztek MA, Nelakurti DD, Brunnuell CL, Mossa-Basha M, Haynor DR, Prevedello LM (2020) Applying artificial intelligence to mitigate effects of patient motion or other complicating factors on image quality. *Top Magn Reson Imaging*. <https://doi.org/10.1097/RMR.0000000000000249>
 216. Nguyen HM, Peng X, Do MN, Liang ZP (2013) Denoising MR spectroscopic imaging data with low-rank approximations. *IEEE Trans Biomed Eng*. <https://doi.org/10.1109/TBME.2012.2223466>
 217. Lam F, Ma C, Liang ZP (2013) Performance analysis of denoising with low-rank and sparsity constraints. *Proc Int Symp Biomed Imaging*. <https://doi.org/10.1109/ISBI.2013.6556701>
 218. Chen Y, Li Y, Xu Z (2020) Improved low-rank filtering of MR spectroscopic imaging data with pre-learned subspace and spatial constraints. *IEEE Trans Biomed Eng*. <https://doi.org/10.1109/TBME.2019.2961698>
 219. Abdoli A, Stoyanova R, Maudsley AA (2016) Denoising of MR spectroscopic imaging data using statistical selection of principal components. *Magn Reson Mater Physics Biol Med*. <https://doi.org/10.1007/s10334-016-0566-z>
 220. Brender JR, Kishimoto S, Merkle H, Reed G, Hurd RE, Chen AP, Ardenkjaer-Larsen JH, Munasinghe J, Saito K, Seki T, Oshima N, Yamamoto K, Choyke PL, Mitchell J, Krishna MC (2019) Dynamic imaging of glucose and lactate metabolism by 13 C-MRS without hyperpolarization. *Sci Rep*. <https://doi.org/10.1038/s41598-019-38981-1>
 221. Mehralivand S, Harmon SA, Shih JH, Smith CP, Lay N, Argun B, Bednarova S, Baroni RH, Canda AE, Ercan K, Girometti R, Karaarslan E, Kural AR, Puryko AS, Rais-Bahrami S, Tonso VM, Magi-Galluzzi C, Gordetsky JB, MacArenco RSES, Merino MJ, Gumuskaya B, Saglican Y, Sioletic S, Warren AY, Barrett T, Bittencourt L, Coskun M, Knauss C, Law YM, Malayeri AA, Margolis DJ, Marko J, Yakar D, Wood BJ, Pinto PA, Choyke PL, Summers RM, Turkbey B (2020) Multicenter multireader evaluation of an artificial intelligence-based attention mapping system for the detection of prostate cancer with multiparametric MRI. *Am J Roentgenol*. <https://doi.org/10.2214/AJR.19.22573>
 222. Tiwari P, Rosen M, Madabhushi A (2009) A hierarchical spectral clustering and nonlinear dimensionality reduction scheme for detection of prostate cancer from magnetic resonance spectroscopy (MRS). *Med Phys* doi 10(1118/1):3180955
 223. Laudadio T, Pels P, De Lathauwer L, Van Hecke P, Van Huffel S (2005) Tissue segmentation and classification of MRSI data using canonical correlation analysis. *Magn Reson Med*. <https://doi.org/10.1002/mrm.20710>
 224. Ion-Mărgineanu A, Kocivar G, Stamile C, Sima DM, Durand-Dubief F, Van Huffel S, Sappey-Marinié D (2017) A comparison of machine learning approaches for classifying multiple sclerosis courses using MRSI and brain segmentations. *Lect Notes Comput Sci*. https://doi.org/10.1007/978-3-319-68612-7_73
 225. Dandil E, Biçer A (2020) Automatic grading of brain tumours using LSTM neural networks on magnetic resonance spectroscopy signals. *IET Image Process*. <https://doi.org/10.1049/iet-ipl.2019.1416>
 226. Acquarelli J, Heerschap A, Postma G, van Laarhoven T, Jansen J, Marchiori E, Buydens L (2018) Classification of brain tumors by 1H MRSI and MRI using convolutional neural networks In: *Proceedings of the 26th scientific meeting, International Society for Magnetic Resonance in medicine, Paris*, p 1325
 227. Green AK, Reeder-Hayes KE, Corty RW, Basch E, Milowsky MI, Dusetzina SB, Bennett AV, Wood WA (2015) The project data sphere initiative: accelerating cancer research by sharing data. *Oncologist*. <https://doi.org/10.1634/theoncologist.2014-0431>
 228. Louis DN, Perry A, Reifenberger G, von Deimling A, Figarella-Branger D, Cavenee WK, Ohgaki H, Wiestler OD, Kleihues P, Ellison DW (2016) The 2016 World Health Organization classification of tumors of the central nervous system: a summary. *Acta Neuropathol*. <https://doi.org/10.1007/s00401-016-1545-1>
 229. Andronesi OC, Rapalino O, Gerstner E, Chi A, Batchelor TT, Cahill DP, Sorensen AG, Rosen BR (2013) Detection of oncogenic IDH1 mutations using magnetic resonance spectroscopy of 2-hydroxyglutarate. *J Clin Invest*. <https://doi.org/10.1172/JCI67229>
 230. Hatano K, Nonomura N (2021) Genomic profiling of prostate cancer: an updated review. *World J Mens Health*. <https://doi.org/10.5534/WJMH.210072>
 231. Eiber M, Weirich G, Holzapfel K, Souvatzoglou M, Haller B, Rauscher I, Beer AJ, Wester HJ, Gschwend J, Schwaiger M, Maurer T (2016) Simultaneous 68Ga-PSMA HBED-CC PET/MRI improves the localization of primary prostate cancer. *Eur Urol*. <https://doi.org/10.1016/j.eururo.2015.12.053>
 232. Savir-Baruch B, Werner RA, Rowe SP, Schuster DM (2021) PET Imaging for prostate cancer. *Radiol Clin North Am*. <https://doi.org/10.1016/j.rcl.2021.05.008>
 233. Siemens Healthineers (2022). <https://www.siemens-healthineers.com/>
 234. Baur ADJ, Hansen CM, Rogasch J, Posch H, Elezkurtaj S, Maxeiner A, Erb-Eigner K, Makowski MR (2020) Evaluation of T1 relaxation time in prostate cancer and benign prostate tissue using a modified look-locker inversion recovery sequence. *Sci Rep*. <https://doi.org/10.1038/s41598-020-59942-z>
 235. Gibbs P, Liney GP, Pickles MD, Zelhof B, Rodrigues G, Turnbull LW (2009) Correlation of ADC and T2 measurements with cell density in prostate cancer at 3.0 Tesla. *Invest Radiol*. <https://doi.org/10.1097/rli.0b013e3181b4c10e>